International Journal of Fracture **82:** 267–295, 1996.

Interaction of newly defined stress intensity factors for angular corners in a row of diamond-shaped inclusions

NAO-AKI NODA[1], YUUJI KAWASHIMA[1], SHINYA MORIYAMA[1] and KAZUHIRO ODA[2]

[1] *Department of Mechanical Engineering, Kyushu Institute of Technology, 1-1 Sensui-cho, Tobata, Kitakyushu 804, Japan; e-mail: noda@mech.kyutech.ac.jp.*

[2] *Department of Mechanical and Electrical Engineering, Tokuyama College of Technology, 3538 Takajo, Kume, Tokuyama 745, Japan; e-mail: oda@tokuyama.ac.jp.*

Received 20 May 1996; accepted in final form 5 September 1996

Abstract. This paper deals with a row of equally spaced equal diamond-shaped inclusions with angular corners under various loading conditions. The problem is formulated as a system of singular integral equations with Cauchy-type singularities, where the unknown functions are the densities of body forces distributed in infinite plates having the same elastic constants of the matrix and inclusions. In order to analyze the problems accurately, the unknown functions of the body force densities are expressed as a linear combination of two types of fundamental density functions and power series, where the fundamental density functions are chosen to represent the symmetric stress singularity of $1/r^{1-\lambda_1}$ and the skew-symmetric stress singularity of $1/r^{1-\lambda_2}$. Then, newly defined stress intensity factors for angular corners are systematically calculated for various shapes, spacings, elastic constants and numbers of the diamond-shaped inclusions in a plate subjected to uniaxial tension, biaxial tension and in-plane shear. For all types of diamond-shaped inclusions, the stress intensity factor is shown to be linearly related to the reciprocal of the number of diamond-shaped inclusions.

Key words: Stress intensity factor, angular corner, diamond-shaped inclusion, singular integral equation, body force method, interface, composite.

1. Introduction

To evaluate the interface strength of composite materials, numerical analyses of stress singularity at the corner of jointed dissimilar materials have been treated in many papers. The stress field of angular corners in dissimilar materials is different from that of ordinary cracks. Recently, Chen and Nisitani [1–5] have indicated that around the corners there appear to be two independent singular stress fields, each corresponding to mode I and mode II type deformation, as shown in Equation (1),

$$\sigma_{ij} = \frac{K_{\mathrm{I},\lambda_1}}{r^{1-\lambda_1}} f_{ij}^{\mathrm{I}}(\theta) + \frac{K_{\mathrm{II},\lambda_2}}{r^{1-\lambda_2}} f_{ij}^{\mathrm{II}}(\theta). \tag{1}$$

In most previous studies, only the stress field with higher singularity has been considered and that leads to wrong conclusions in some cases; namely, both different types of stress singularities have to be taken into account to evaluate the interface strength of dissimilar materials [3].

In our previous papers, the numerical solution for singular integral equations of the body force method is considered; the unknown functions are approximated by the products of fundamental density functions and polynomials [6, 7]. In our last paper, a row of diamond-shaped holes has been accurately analyzed [8]; through the study, the effectiveness of the

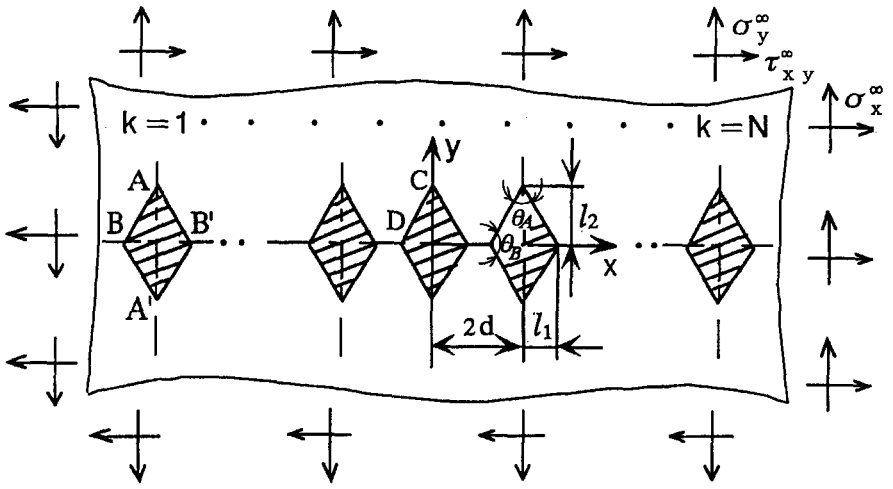

Figure 1. Diamond-shaped inclusions in an infinite plate.

numerical solution for the newly defined stress intensity factors for angular corners has been clarified.

In this paper, interaction of diamond-shaped inclusions is considered. This shape of inclusion is regarded as a basic model when the new stress intensity factor for angular corners is applied to the evaluation of dissimilar materials. For example, when both the corner angle and elastic modulus of inclusions approach zero, the present results should coincide with the ones of ordinary cracks [9]. Figure 1 shows the problem treated in this paper, that is, a row of diamond-shaped inclusions in an infinite plate subjected to three fundamental loads; (1) uniaxial tension, (2) biaxial tension and (3) in-plane shear at infinity.

2. Numerical solutions for singular integral equations for a row of diamond-shaped inclusions

Consider a row of diamond-shaped inclusions with the same configuration in an infinite plate (Figure 1). Here, l_1 and l_2 are sizes of inclusions, d is a parameter of distance, θ_A and θ_B are angles of the corner A and B, respectively and σ_x^∞, σ_y^∞ and τ_{xy}^∞ are stresses at infinity. Denote the shear modulus and Poisson's ratios of the matrix by G_1, ν_1 and the inclusions by G_2, ν_2.

In this analysis, body forces distributed along the imaginary boundary in an infinite plate are expressed as a sum of two types of distribution of body forces. The body forces acting in the normal direction (θ-direction) and the tangential direction (r-direction) are expressed as two types, that is, symmetric (mode I) and skew-symmetric (mode II) types to the bisector of the corners. They can express mode I and mode II types of deformations that occur at the corner [3, 7, 8].

As shown in Figure 2, in order to obtain the relationship between the tractions $(\sigma_{nM,i}, \tau_{ntM,i})$ and displacements $(u_{M,i}, v_{M,i})$ on the boundary of the ith diamond-shaped hole in an infinite plate containing a row of diamond-shaped holes (the number of holes is N), the body forces are distributed in the θ- and r-directions on the prospective boundary of the kth diamond-shaped hole in an infinite plate 'M', which has the same elastic constants of the matrix (G_1, ν_1). Then, the body forces are expressed as $F_{\theta M,k}(r_k) = F^{\mathrm{I}}_{\theta M,k}(r_k) + F^{\mathrm{II}}_{\theta M,k}(r_k)$

and $F_{rM,k}(r_k) = F^{\mathrm{I}}_{rM,k}(r_k) + F^{\mathrm{II}}_{rM,k}(r_k)$, where the superscripts I and II denote the distribution types of mode I and mode II, respectively. In a similar way, in order to obtain the relationship between the tractions $(\sigma_{n\mathrm{I},i}, \tau_{nt\mathrm{I},i})$ and displacements $(u_{\mathrm{I},i}, v_{\mathrm{I},i})$ on the boundary of the ith diamond-shaped inclusion, the body forces are distributed in the θ- and r-directions on the prospective boundary of the kth diamond-shaped inclusion in an infinite plate 'I', which has the same elastic constants of the inclusions; then the body forces are expressed as $F_{\theta I,k}(r_k) = F^{\mathrm{I}}_{\theta I,k}(r_k) + F^{\mathrm{II}}_{\theta I,k}(r_k)$ and $F_{rI,k}(r_k) = F^{\mathrm{I}}_{rI,k}(r_k) + F^{\mathrm{II}}_{rI,k}(r_k)$. In this way, a system of singular integral equations that express the boundary conditions ($\sigma_{nM,i} - \sigma_{nI,i} = 0, \tau_{ntM,i} - \tau_{ntI,i} = 0, u_{M,i} - u_{I,i} = 0$ and $v_{M,i} - v_{I,i} = 0$) on the boundary containing the corner is shown in Equations (2) and (3)

$$
\begin{aligned}
&-\tfrac{1}{2}F_{\theta M,i}(s_i) - \tfrac{1}{2}F_{\theta I,i}(s_i) \\
&\quad + \sum_{k=1}^{N}\left[\int_{L_k} h_{nm}^{F_{\theta M,k}}(r_k, s_i)F_{\theta M,k}(r_k)\,\mathrm{d}r_k + \int_{L_k} h_{nn}^{F_{rM,k}}(r_k, s_i)F_{rM,k}(r_k)\,\mathrm{d}r_k\right. \\
&\qquad \left. - \int_{L_k} h_{nn}^{F_{\theta I,k}}(r_k, s_i)F_{\theta I,k}(r_k)\,\mathrm{d}r_k - \int_{L_k} h_{nn}^{F_{rI,k}}(r_k, s_i)F_{rI,k}(r_k)\,\mathrm{d}r_k\right] \\
&\quad = -\sigma^{\infty}_{nM}(s_i) + \sigma^{\infty}_{nI}(s_i),
\end{aligned}
\tag{2}
$$

$$
\begin{aligned}
&-\tfrac{1}{2}F_{rM,i}(s_i) - \tfrac{1}{2}F_{rI,i}(s_i) \\
&\quad + \sum_{k=1}^{N}\left[\int_{L_k} h_{nt}^{F_{\theta M,k}}(r_k, s_i)F_{\theta M,k}(r_k)\,\mathrm{d}r_k + \int_{L_k} h_{nt}^{F_{rM,k}}(r_k, s_i)F_{rM,k}(r_k)\,\mathrm{d}r_k\right. \\
&\qquad \left. - \int_{L_k} h_{nt}^{F_{\theta I,k}}(r_k, s_i)F_{\theta I,k}(r_k)\,\mathrm{d}r_k - \int_{L_k} h_{nt}^{F_{rI,k}}(r_k, s_i)F_{rI,k}(r_k)\,\mathrm{d}r_k\right] \\
&\quad = -\tau^{\infty}_{ntM}(s_i) + \tau^{\infty}_{ntI}(s_i) \quad (i = 1 \sim N),
\end{aligned}
$$

$$
\begin{aligned}
&\sum_{k=1}^{N}\left[\int_{L_k} h_{u}^{F_{\theta M,k}}(r_k, s_i)F_{\theta M,k}(r_k)\,\mathrm{d}r_k + \int_{L_k} h_{u}^{F_{rM,k}}(r_k, s_i)F_{rM,k}(r_k)\,\mathrm{d}r_k\right. \\
&\qquad \left. - \int_{L_k} h_{u}^{F_{\theta I,k}}(r_k, s_i)F_{\theta I,k}(r_k)\,\mathrm{d}r_k - \int_{L_k} h_{u}^{F_{rI,k}}(r_k, s_i)F_{rI,k}(r_k)\,\mathrm{d}r_k\right] \\
&\quad = -u^{\infty}_{M,i} + u^{\infty}_{I,i},
\end{aligned}
\tag{3}
$$

$$
\sum_{k=1}^{N}\left[\int_{L_k} h_{v}^{F_{\theta M,k}}(r_k, s_i)F_{\theta M,k}(r_k)\,\mathrm{d}r_k + \int_{L_k} h_{v}^{F_{rM,k}}(r_k, s_i)F_{rM,k}(r_k)\,\mathrm{d}r_k\right.
$$

$$-\int_{L_k} h_v^{F_{\theta I,k}}(r_k, s_i) F_{\theta I,k}(r_k)\,\mathrm{d}r_k - \int_{L_k} h_v^{F_{rI,k}}(r_k, s_i) F_{rI,k}(r_k)\,\mathrm{d}r_k\Bigg]$$

$$= -v_{M,i}^{\infty} + v_{I,i}^{\infty} \quad (i = 1 \sim N).$$

Here, $\Sigma_{k=1}^{N}$ means the sum total of the prospective boundary of each diamond-shaped hole and inclusion. The notation $\int_{L_k}$ means integrating the body forces on the boundary of the kth diamond-shaped hole (plate M) or inclusion (plate I). The notations $\sigma_{n,M}^{\infty}(s_i)$ and $\tau_{ntM}^{\infty}(s_i)$ mean normal and shear stresses appear at the point s_i in plate M. Taking $h_{nn}^{F_{\theta M,k}}(r_k, s_i)$ as an example, the notation means the normal stress induced at the collocation point s_i on the imaginary boundary of the ith diamond-shaped hole when the body force with unit density in the θ-direction is acting at the point r_k on the prospective boundary of the kth diamond-shaped hole. The body forces are symmetrically and skew-symmetrically distributed with respect to the y-axis. In this study, in order to analyze Equations (2) and (3) accurately, the side of the diamond-shaped hole or inclusion is divided into four parts; then, on each part the distributed body force densities are approximated by a linear combination of power series ($W_{\theta M,k}^{\mathrm{I}} \sim W_{rI,k}^{\mathrm{II}}$) and two fundamental density functions, that is, $r_k^{\lambda_1 - 1}$ (distribution density of a symmetric type to the bisector of the corner) and $r_k^{\lambda_2 - 1}$ (distribution density of a skew-symmetric type to the bisector of the corner) as shown in Equation (4). In the following equations, the numerical solution will be shown by taking an example for the corner A. Here, $r_{A,k}$ is a distance measured from the corner A.

$$\begin{aligned}
F_{\theta AM,k}(r_{A,k}) &= F_{\theta AM,k}^{\mathrm{I}}(r_{A,k}) + F_{\theta AM,k}^{\mathrm{II}}(r_{A,k}) \\
&= W_{\theta AM,k}^{\mathrm{I}}(r_{A,k}) r_{A,k}^{\lambda_1 - 1} + W_{\theta AM,k}^{\mathrm{II}}(r_{A,k}) r_{A,k}^{\lambda_2 - 1}, \\
F_{rAM,k}(r_{A,k}) &= F_{rAM,k}^{\mathrm{I}}(r_{A,k}) + F_{rAM,k}^{\mathrm{II}}(r_{A,k}) \\
&= W_{rAM,k}^{\mathrm{I}}(r_{A,k}) r_{A,k}^{\lambda_1 - 1} + W_{rAM,k}^{\mathrm{II}}(r_{A,k}) r_{A,k}^{\lambda_2 - 1}, \\
F_{\theta AI,k}(r_{A,k}) &= F_{\theta AI,k}^{\mathrm{I}}(r_{A,k}) + F_{\theta AI,k}^{\mathrm{II}}(r_{A,k}) \\
&= W_{\theta AI,k}^{\mathrm{I}}(r_{A,k}) r_{A,k}^{\lambda_1 - 1} + W_{\theta AI,k}^{\mathrm{II}}(r_{A,k}) r_{A,k}^{\lambda_2 - 1}, \\
F_{rAI,k}(r_{A,k}) &= F_{rAI,k}^{\mathrm{I}}(r_{A,k}) + F_{rAI,k}^{\mathrm{II}}(r_{A,k}) \\
&= W_{rAI,k}^{\mathrm{I}}(r_{A,k}) r_{A,k}^{\lambda_1 - 1} + W_{rAI,k}^{\mathrm{II}}(r_{A,k}) r_{A,k}^{\lambda_2 - 1},
\end{aligned} \tag{4}$$

$$
\begin{aligned}
W^{\mathrm{I}}_{\theta AM,k}(r_{A,k}) &= \sum_{n=1}^{M} a_{n,k} r_{A,k}^{n-1}, & W^{\mathrm{I}}_{rAM,k}(r_{A,k}) &= \sum_{n=1}^{M} b_{n,k} r_{A,k}^{n-1}, \\
W^{\mathrm{II}}_{\theta AM,k}(r_{A,k}) &= \sum_{n=1}^{M} c_{n,k} r_{A,k}^{n-1}, & W^{\mathrm{II}}_{rAM,k}(r_{A,k}) &= \sum_{n=1}^{M} d_{n,k} r_{A,k}^{n-1}, \\
W^{\mathrm{I}}_{\theta AI,k}(r_{A,k}) &= \sum_{n=1}^{M} e_{n,k} r_{A,k}^{n-1}, & W^{\mathrm{I}}_{rAI,k}(r_{A,k}) &= \sum_{n=1}^{M} f_{n,k} r_{A,k}^{n-1}, \\
W^{\mathrm{II}}_{\theta AI,k}(r_{A,k}) &= \sum_{n=1}^{M} g_{n,k} r_{A,k}^{n-1}, & W^{\mathrm{II}}_{rAI,k}(r_{A,k}) &= \sum_{n=1}^{M} h_{n,k} r_{A,k}^{n-1}.
\end{aligned}
\tag{5}
$$

Here, the eigenvalues λ_1 and λ_2 are given as the roots of the following eigenequations (see Figure 3) [1, 2]

$$
\begin{aligned}
&(\alpha-\beta)^2\lambda_1^2(1-\cos 2\gamma) + 2\lambda_1(\alpha-\beta)\sin\gamma \\
&\quad\times\{\sin\lambda_1\gamma + \sin\lambda_1(2\pi-\gamma)\} + 2\lambda_1(\alpha-\beta)\beta\sin\gamma \\
&\quad\times\{\sin\lambda_1(2\pi-\gamma) - \sin\lambda_1\gamma\} + (1-\alpha^2) - (1-\beta^2)\cos 2\lambda_1\pi \\
&\quad+(\alpha^2-\beta^2)\cos\{2\lambda_1(\gamma-\pi)\} = 0,
\end{aligned}
\tag{6}
$$

for mode I and

$$
\begin{aligned}
&(\alpha-\beta)^2\lambda_2^2(1-\cos 2\gamma) - 2\lambda_2(\alpha-\beta)\sin\gamma \\
&\quad\times\{\sin\lambda_2\gamma + \sin\lambda_2(2\pi-\gamma)\} - 2\lambda_2(\alpha-\beta)\beta\sin\gamma \\
&\quad\times\{\sin\lambda_2(2\pi-\gamma) - \sin\lambda_2\gamma\} + (1-\alpha^2) - (1-\beta^2)\cos 2\lambda_2\pi \\
&\quad+(\alpha^2-\beta^2)\cos\{2\lambda_2(\gamma-\pi)\} = 0,
\end{aligned}
\tag{7}
$$

for mode II, where α and β are Dundurs' composite parameters and are related to the elastic constants of each constituent by

$$
\alpha = \frac{G_1(\kappa_2+1) - G_2(\kappa_1+1)}{G_1(\kappa_2+1) + G_2(\kappa_1+1)}, \qquad \beta = \frac{G_1(\kappa_2-1) - G_2(\kappa_1-1)}{G_1(\kappa_2+1) + G_2(\kappa_1+1)},
$$

where

$$
\kappa_j = \begin{cases} (3-\nu_j)/(1+\nu_j) & \text{(plane stress)} \\ 3-4\nu_j & \text{(plane strain)} \end{cases} \qquad (j=1,2).
$$

In a similar way, the body forces distributed around other corners are also represented. By using the numerical method mentioned above, the integral equations are solved and the unknown coefficients $a_{n,k} \sim h_{n,k}$ are determined so as to satisfy the boundary conditions at the suitably chosen collocation points. The stress intensity factors $K_{\mathrm{I},\lambda_1,k}$, $K_{\mathrm{II},\lambda_2,k}$ for the angular corner A

of the kth diamond-shaped inclusion defined by Equation (1) can be obtained from the values of $W^{\mathrm{I}}_{\theta AM,k}(0), W^{\mathrm{II}}_{\theta AM,k}(0), W^{\mathrm{I}}_{rAM,k}(0)$ and $W^{\mathrm{II}}_{rAM,k}(0)$ at the corner tip by Equation (8) and (9).

$$
\begin{aligned}
K_{\mathrm{I},\lambda_1,k} = {} & \frac{1}{\lambda_1} \times \frac{-2\sqrt{2\pi}(\alpha-\beta)(\kappa_1 q_7 + \lambda_1 q_1)}{2[\{\lambda_1(\alpha-\beta)q_4 + (1-\beta)q_2\}p_5 + \{(\lambda_1+1)(\alpha-\beta)q_3\}p_6]} \\
& \overline{\times(\kappa_1 q_7 + \lambda_1 q_1) - [\{\lambda_1(\alpha-\beta)q_4 + (1-\beta)q_2\}p_5} \\
& \overline{+\{(\lambda_1-\kappa_1)(\alpha-\beta)q_3\}p_6] \times [(\kappa_1-1)q_7 + (\kappa_1+2\lambda_1+1)q_1]} \\
& \overline{+[\{\lambda_1(\alpha-\beta)q_4 + (1-\beta)q_2\}q_5 + \{(\lambda_1+\kappa_1)(\alpha-\beta)q_3\}q_6]} \\
& \overline{\times(\kappa_1+1)(p_7+p_1)} \times W^{\mathrm{I}}_{\theta AM,k}(0), \\
K_{\mathrm{I},\lambda_1,k} = {} & \frac{1}{\lambda_1} \times \frac{-2\sqrt{2\pi}(\alpha-\beta)(\kappa_1 q_7 + \lambda_1 q_1)}{2[\{\lambda_1(\alpha-\beta)q_4 + (1-\beta)q_2\}q_5 + \{(\lambda_1-1)(\alpha-\beta)q_3\}q_6]} \\
& \overline{\times(\kappa_1 q_7 + \lambda_1 q_1) - [\{\lambda_1(\alpha-\beta)q_4 + (1-\beta)q_2\}p_5} \\
& \overline{+\{(\lambda_1-\kappa_1)(\alpha-\beta)q_3\}p_6] \times (\kappa_1+1)(p_7-p_1) + [\{\lambda_1(\alpha-\beta)q_4} \\
& \overline{+(1-\beta)q_2\}q_5 + \{(\lambda_1+\kappa_1)(\alpha-\beta)q_3\}q_6][(1-\kappa_1)q_7} \\
& \overline{+(\kappa_1-2\lambda_1+1)q_1]} \times W^{\mathrm{I}}_{rAM,k}(0),
\end{aligned}
\tag{8}
$$

$$\gamma = 2\pi - \theta_A,$$

$$p_1 = \cos\gamma, \qquad p_2 = \cos(\lambda_1\pi), \qquad p_3 = \cos[\lambda_1(\gamma-\pi)],$$

$$p_4 = \cos[\gamma - \lambda_1(\gamma-\pi)], \qquad p_5 = \cos\frac{(\lambda_1+1)\gamma}{2},$$

$$p_6 = \cos\frac{(\lambda_1-1)\gamma}{2}, \qquad p_7 = \cos(2\lambda_1\pi - \lambda_1\gamma),$$

$$q_1 = \sin\gamma, \qquad q_2 = \sin(\lambda_1\pi), \qquad q_3 = \sin[\lambda_1(\gamma-\pi)],$$

$$q_4 = \sin[\gamma - \lambda_1(\gamma-\pi)], \qquad q_5 = \sin\frac{(\lambda_1+1)\gamma}{2},$$

$$q_6 = \sin\frac{\lambda_1-1)\gamma}{2}, \qquad q_7 = \sin(2\lambda_1\pi - \lambda_1\gamma),$$

$$
\begin{aligned}
K_{\mathrm{II},\lambda_2,k} = {} & \frac{1}{\lambda_2} \times \frac{2\sqrt{2\pi}(\alpha-\beta)(\kappa_1 q_{13} - \lambda_2 q_1)}{2[\{\lambda_2(\alpha-\beta)q_{10} - (1-\beta)q_8\}q_{11} + \{(\lambda_2+1)(\alpha-\beta)q_9\}q_{12}]} \\
& \overline{\times(\kappa_1 q_{13} - \lambda_2 q_1) - [\{\lambda_2(\alpha-\beta)q_{10} - (1-\beta)q_8\}q_{11}} \\
& \overline{+\{(\lambda_2-\kappa_1)(\alpha-\beta)q_9\}q_{12}] \times [(1-\kappa_1)q_{13} + (\kappa_1+2\lambda_2+1)q_1]} \\
& \overline{+[\{\lambda_2(\alpha-\beta)q_{10} - (1-\beta)q_8\}p_{11} + \{(\lambda_2+\kappa_1)(\alpha-\beta)q_9\}p_{12}]} \\
& \overline{\times(\kappa_1+1)(p_{13}-p_1)} \times W^{\mathrm{II}}_{\theta AM,k}(0), \\
K_{\mathrm{II},\lambda_2,k} = {} & \frac{1}{\lambda_2} \times \frac{2\sqrt{2\pi}(\alpha-\beta)(\kappa_1 q_{13} - \lambda_2 q_1)}{2[\{\lambda_2(\alpha-\beta)q_{10} - (1-\beta)q_8\}p_{11} + \{(\lambda_2-1)(\alpha-\beta)q_9\}p_{12}]} \\
& \overline{\times(\kappa_1 q_{13} - \lambda_2 q_1) + [\{\lambda_2(\alpha-\beta)q_{10} - (1-\beta)q_8\}q_{11}} \\
& \overline{+\{(\lambda_2-\kappa_1)(\alpha-\beta)q_9\}q_{12}] \times [(\kappa_1+1)(p_{13}+p_1) + [\{\lambda_2(\alpha-\beta)q_{10}} \\
& \overline{-(1-\beta)q_8\}p_{11} + \{(\lambda_2+\kappa_1)(\alpha-\beta)q_9\}p_{12}]} \\
& \overline{\times[(\kappa_1-1)q_{13} + (\kappa_1-2\lambda_2+1)q_1]} \times W^{\mathrm{II}}_{rAM,k}(0),
\end{aligned}
\tag{9}
$$

$$
\gamma = 2\pi - \theta_A,
$$

$$
p_1 = \cos\gamma, \qquad p_8 = \cos(\lambda_2\pi), \qquad p_9 = \cos[\lambda_2(\gamma-\pi)],
$$

$$
p_{10} = \cos[\gamma - \lambda_2(\gamma-\pi)], \qquad p_{11} = \cos\frac{(\lambda_2+1)\gamma}{2},
$$

$$
p_{12} = \cos\frac{(\lambda_2-1)\gamma}{2}, \qquad p_{13} = \cos(2\lambda_2\pi - \lambda_2\gamma),
$$

$$
q_1 = \sin\gamma, \qquad q_8 = \sin(\lambda_2\pi), \qquad q_9 = \sin[\lambda_2(\gamma-\pi)],
$$

$$
q_{10} = \sin[\gamma - \lambda_2(\gamma-\pi)], \qquad q_{11} = \sin\frac{(\lambda_2+1)\gamma}{2},
$$

$$
q_{12} = \sin\frac{(\lambda_2-1)\gamma}{2}, \qquad q_{13} = \sin(2\lambda_2\pi - \lambda_2\gamma).
$$

3. Results and discussion

In Figure 1, stress intensity factors $K_{\mathrm{I},\lambda_1,k}$ and $K_{\mathrm{II},\lambda_2,k}$ defined at corners A, B, B', C, D are analyzed with varying geometrical parameters $\theta_A, \theta_B, l_1/d, l_2/d$, elastic ratio G_2/G_1, and number of inclusions N systematically. Table 1 and Table 2 show the values of λ_1 and λ_2 in the case of plane strain and $\nu_1 = \nu_2 = 0.3$ treated in this analysis.

First, the accuracy of the present method for these problems is examined. The values of $K_{\mathrm{I},\lambda_1,k}$ can be determined from the values $W^{\mathrm{I}}_{\theta,k}(0), W^{\mathrm{I}}_{r,k}(0)$, and the values $K_{\mathrm{II},\lambda_2,k}$ from

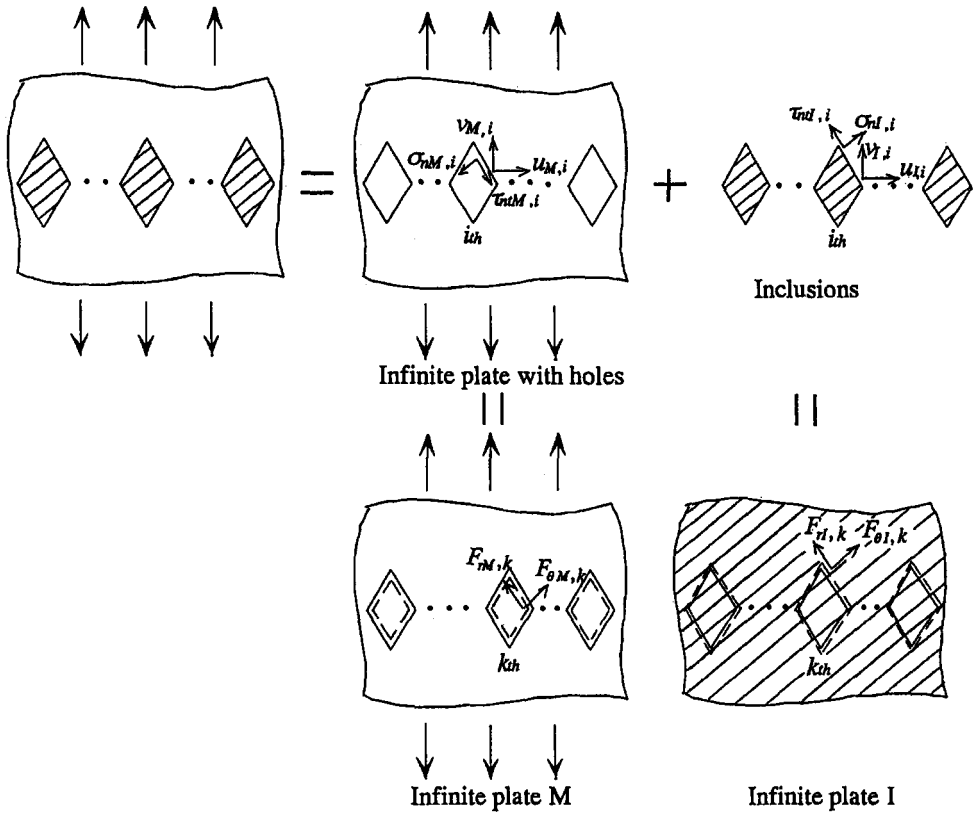

Figure 2. Formulation of the singular integral equation based on the body force method.

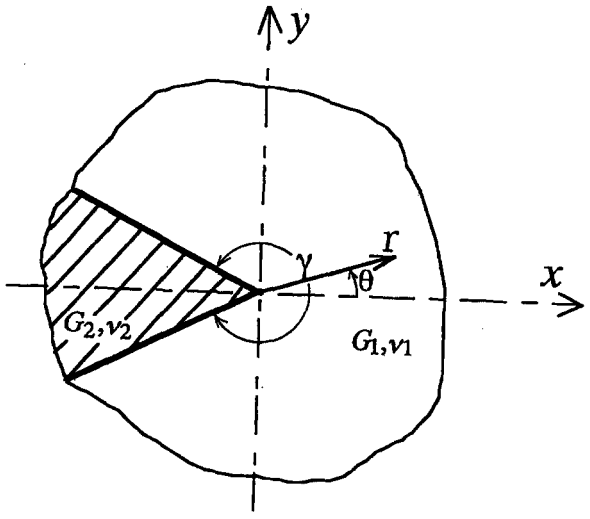

Figure 3. Corner of two bonded wedges.

$W^{\mathrm{II}}_{\theta,k}(0), W^{\mathrm{II}}_{r,k}(0)$. Those values of $K_{\mathrm{I},\lambda_1,k}$ (or $K_{\mathrm{II},\lambda_2,k}$) obtained from two weight functions $W^{\mathrm{I}}_{\theta,k}(0), W^{\mathrm{I}}_{r,k}(0)$ (or $W^{\mathrm{II}}_{\theta,k}(0), W^{\mathrm{II}}_{r,k}(0)$) should be in agreement within the error of numerical

Table 1. λ_1 corresponding to mode I. (Plane strain state $\nu_1 = \nu_2 = 0.3$)

G_2/G_1 θ_A, θ_B	10^{-5}	10^{-2}	10^{-1}	10^{1}	10^{2}	10^{5}
30°	0.5014531	0.5529604	0.7851341	0.6822381	0.5862285	0.5732316
60°	0.5122214	0.5362765	0.6900333	0.7219039	0.6684683	0.6619053
90°	0.5444838	0.5583162	0.6601418	0.7981112	0.7632349	0.7590462
120°	0.6157311	0.6243555	0.6920671	0.8755021	0.8533334	0.8506666
150°	0.7519746	0.7569233	0.7967322	0.9408892	0.9296663	0.9283023

Table 2. λ_2 corresponding to mode II. (Plane strain state $\nu_1 = \nu_2 = 0.3$)

G_2/G_1 θ_A, θ_B	10^{-5}	10^{-2}	10^{-1}	10^{1}	10^{2}	10^{5}
30°	0.5981919	0.6143511	0.7239281	—	—	0.5210558
60°	0.7309007	0.7382624	0.7940938	—	0.6359865	0.5490489
90°	0.9085292	0.9116800	0.9355639	0.7856547	0.6218440	0.5951843
120°	—	—	—	0.7614816	0.6824355	0.6714777
150°	—	—	—	0.8379280	0.8010302	0.7962951

calculation. Tables 3 and 4 show examples with different numbers of collocation points. In Table 3, dimensionless stress intensity factors $F_{\mathrm{I},\lambda_1,k}$ and $F_{\mathrm{II},\lambda_2,k}$ at the corner A of the outermost diamond-shaped inclusion are tabulated, whose values are obtained from the Equation (10) when $N = 4, \nu_1 = \nu_2 = 0.3, \theta_A = 60°, l_2/d = \frac{1}{2}, G_2/G_1 = 10^{-1}$ under biaxial tension ($\sigma_x^\infty = \sigma_y^\infty = \sigma^\infty, \tau_{xy}^\infty = 0$) and plane strain.

$$F_{\mathrm{I},\lambda_1,k} = \frac{K_{\mathrm{I},\lambda_1,k}}{\sigma^\infty \sqrt{\pi} l_2^{1-\lambda_1}}, \qquad F_{\mathrm{II},\lambda_2,k} = \frac{K_{\mathrm{II},\lambda_2,k}}{\sigma^\infty \sqrt{\pi} l_2^{1-\lambda_2}}. \tag{10}$$

On the other hand, Table 4 shows convergency of the $F_{\mathrm{I},\lambda_1,k}$ and $F_{\mathrm{II},\lambda_2,k}$ at the corner C of the middle diamond-shaped inclusion obtained from Equation (11) when $N = 4, \nu_1 = \nu_2 = 0.3, \theta_A = 60°, l_2/d = \frac{1}{2}, G_2/G_1 = 10^{-1}$ under in-plane shear ($\tau_{xy}^\infty = \tau^\infty, \sigma_x^\infty = \sigma_y^\infty = 0$) and plane strain.

$$F_{\mathrm{I},\lambda_1,k} = \frac{K_{\mathrm{I},\lambda_1,k}}{\tau^\infty \sqrt{\pi} l_2^{1-\lambda_1}}, \qquad F_{\mathrm{II},\lambda_2,k} = \frac{K_{\mathrm{II},\lambda_2,k}}{\tau^\infty \sqrt{\pi} l_2^{1-\lambda_2}}. \tag{11}$$

Here, M is the collocation number in the vicinity of the corner, the total collocation number is $4MN$ and the number of algebraic equations to obtain the unknown functions is $16MN$. The results of Table 3 and Table 4 have good convergency. Results of other inclusion corners and other geometrical and loading conditions are also examined; then, the present method is found to yield rapidly converging numerical results. Furthermore, the values obtained from different weight functions of the body forces in θ- and r-directions coincide with each other in about four digits when $M = 12$ through the present method.

Table 5 shows the intensity factors (F_{I,λ_1} and $F_{\mathrm{II},\lambda_2}$) at the corner $A(\theta_A \leq 90°)$ when $N = 2$ with varying parameters $\theta_A, l_2/d, G_2/G_1$. Here, three kinds of fundamental loads at

Table 3. Convergency of $F_{\mathrm{I},\lambda_1,k}$ and $F_{\mathrm{II},\lambda_2,k}$ at the corner A. ($N = 4, \nu_1 = \nu_2 = 0.3, \theta_A = 60°, l_2/d = \frac{1}{2}, G_2/G_1 = 10^{-1}, \sigma_x^\infty = \sigma_y^\infty = \sigma^\infty, \tau_{xy}^\infty = 0$, plane strain state in Figure 1)

	$F_{\mathrm{I},\lambda_1,k}(\lambda_1 = 0.6900333)$		$F_{\mathrm{II},\lambda_2,k}(\lambda_2 = 0.7940938)$	
M	from $W^{\mathrm{I}}_{\theta,k}(0)$	from $W^{\mathrm{I}}_{r,k}(0)$	from $W^{\mathrm{II}}_{\theta,k}(0)$	from $W^{\mathrm{II}}_{r,k}(0)$
4	0.61869	0.61850	0.01887	0.01887
6	0.61904	0.61891	0.01890	0.01890
8	0.61915	0.61907	0.01891	0.01891
10	0.61919	0.61913	0.01892	0.01892
12	0.61918	0.61915	0.01892	0.01892

Table 4. Convergency of $F_{\mathrm{I},\lambda_1,k}$ and $F_{\mathrm{II},\lambda_2,k}$ at the corner C. ($N = 4, \nu_1 = \nu_2 = 0.3, \theta_A = 60°, l_2/d = \frac{1}{2}, G_2/G_1 = 10^{-1}, \tau_{xy}^\infty = \tau^\infty, \sigma_x^\infty = \sigma_y^\infty = 0$, plane strain state in Figure 1)

	$F_{\mathrm{I},\lambda_1,k}(\lambda_1 = 0.6900333)$		$F_{\mathrm{II},\lambda_2,k}(\lambda_2 = 0.7940938)$	
M	from $W^{\mathrm{I}}_{\theta,k}(0)$	from $W^{\mathrm{I}}_{r,k}(0)$	from $W^{\mathrm{II}}_{\theta,k}(0)$	from $W^{\mathrm{II}}_{r,k}(0)$
4	0.00377	0.00378	1.58761	1.58762
6	0.00376	0.00377	1.58789	1.58789
8	0.00376	0.00377	1.58798	1.58798
10	0.00376	0.00377	1.58801	1.58801
12	0.00377	0.00377	1.58806	1.58806

infinity, that is, (a) uniaxial tension, (b) biaxial tension and (c) in-plane shear are treated. The value in parenthesis ( ) shows the ratio to the stress intensity factors of a single inclusion. In Table 6, F_{I,λ_1} and $F_{\mathrm{II},\lambda_2}$ at the corners B and $B'(\theta_B \leq 90°)$ under three types of loads are shown. Chen and Nisitani's results of a single inclusion (rigid body or hole) [2] coincide with the present results in four digits. Figures 4 and 5 show the relation between the stress intensity factors and l_1/d when the interaction appears largely. In Figure 4, F_{I,λ_1} increases by about fifty percent when $l_1/d = \frac{2}{3}$ at the corner B' in uniaxial tension (y-direction), $\theta_B = 90°$ and $G_2/G_1 > 1$, even though the absolute values of stress intensity factors are small. In Figure 5, $F_{\mathrm{II},\lambda_2}$ increases by about forty percent at the corner B' under in-plane shear, $\theta_B = 90°$ and $G_2/G_1 < 1$ with the large absolute values of stress intensity factors. In other cases, the interaction effects are not very large and approximately less than twenty percent when $l_1/d \leq \frac{2}{3}$ and $l_2/d \leq \frac{2}{3}$.

Figure 6 shows the relationship between the number of inclusions N and $F_{\mathrm{I},\lambda_1,k}$ values at the corner D at the central inclusion when $\theta_B = 30°, G_2/G_1 = 10^2$ under uniaxial tension (y-direction). As shown in Figure 6, $F_{\mathrm{I},\lambda_1,k}$ and $F_{\mathrm{II},\lambda_2,k}$ are found to be almost linear to $1/N$ for any fixed values of l_1/d or l_2/d. These relations are similar to the parallel and colinear cracks [9] and a row of diamond-shaped holes [8].

Table 5a. F_{I,λ_1} and $F_{\mathrm{II},\lambda_2}$ for two diamond-shaped inclusions at the corner A under various loading conditions. (Plane strain state $\nu_1 = \nu_2 = 0.3$)

(a) Uniaxial tension

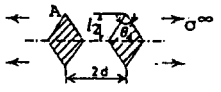

		$F_{\mathrm{I},\lambda_1}(F_{\mathrm{I},\lambda_1}/F_{\mathrm{I},\lambda_1}\|_{l_2/d=0})$						$F_{\mathrm{II},\lambda_2}$					
G_2/G_1		10^{-5}	10^{-2}	10^{-1}	10^{1}	10^{2}	10^{5}	10^{-5}	10^{-2}	10^{-1}	10^{1}	10^{2}	10^{5}
θ_A	l_2/d												
30°	0	1.042	0.909	0.747	−0.160	−0.174	−0.177	0.000	0.000	0.000	—	—	0.000
		(1.000)	(1.000)	(1.000)	(1.000)	(1.000)	(1.000)						
	1/3	0.999	0.878	0.735	−0.161	−0.175	−0.179	0.009	0.008	0.004	—	—	0.009
		(0.959)	(0.966)	(0.984)	(1.006)	(1.006)	(1.011)						
	1/2	0.960	0.848	0.725	−0.162	−0.176	−0.180	0.026	0.022	0.011	—	—	0.022
		(0.921)	(0.933)	(0.971)	(1.013)	(1.011)	(1.017)						
	2/3	0.923	0.820	0.715	−0.162	−0.176	−0.181	0.048	0.042	0.020	—	—	0.035
		(0.886)	(0.902)	(0.957)	(1.013)	(1.011)	(1.023)						
60°	0	1.148	1.054	0.717	−0.154	−0.173	−0.175	0.000	0.000	0.000	—	0.000	0.000
		(1.000)	(1.000)	(1.000)	(1.000)	(1.000)	(1.000)						
	1/3	1.096	1.010	0.698	−0.159	−0.175	−0.177	0.018	0.017	0.010	—	0.002	0.004
		(0.955)	(0.958)	(0.974)	(1.032)	(1.012)	(1.011)						
	1/2	1.049	0.970	0.681	−0.161	−0.176	−0.178	0.049	0.045	0.028	—	0.007	0.012
		(0.914)	(0.920)	(0.950)	(1.045)	(1.017)	(1.017)						
	2/3	1.006	0.933	0.666	−0.161	−0.176	−0.179	0.088	0.082	0.052	—	0.016	0.023
		(0.876)	(0.885)	(0.929)	(1.045)	(1.017)	(1.023)						
90°	0	1.293	1.223	0.858	−0.131	−0.148	−0.152	0.000	0.000	0.000	0.000	0.000	0.000
		(1.000)	(1.000)	(1.000)	(1.000)	(1.000)	(1.000)						
	1/3	1.228	1.163	0.828	−0.145	−0.159	−0.161	0.067	0.065	0.051	0.006	0.006	0.003
		(0.950)	(0.951)	(0.965)	(1.107)	(1.074)	(1.059)						
	1/2	1.172	1.113	0.803	−0.147	−0.161	−0.164	0.177	0.171	0.138	0.020	0.018	0.011
		(0.906)	(0.910)	(0.936)	(1.122)	(1.088)	(1.079)						
	2/3	1.125	1.070	0.781	−0.146	−0.160	−0.165	0.305	0.297	0.244	0.043	0.042	0.026
		(0.870)	(0.875)	(0.910)	(1.115)	(1.081)	(1.086)						

Table 5b. F_{I,λ_1} and $F_{\mathrm{II},\lambda_2}$ for two diamond-shaped inclusions at the corner A under various loading conditions. (Plane strain state $\nu_1 = \nu_2 = 0.3$)

(b) Biaxial tension

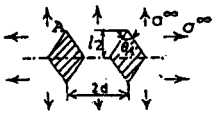

		F_{I,λ_1} ($F_{\mathrm{I},\lambda_1}/F_{\mathrm{I},\lambda_1}\vert_{l_2/d=0}$)						$F_{\mathrm{II},\lambda_2}$					
G_2/G_1		10^{-5}	10^{-2}	10^{-1}	10^{1}	10^{2}	10^{5}	10^{-5}	10^{-2}	10^{-1}	10^{1}	10^{2}	10^{5}
θ_A	l_2/d												
30°	0	1.014 (1.000)	0.889 (1.000)	0.749 (1.000)	0.214 (1.000)	0.244 (1.000)	0.251 (1.000)	0.000	0.000	0.000	—	—	0.000
	1/3	0.977 (0.964)	0.862 (0.970)	0.740 (0.988)	0.213 (0.995)	0.243 (0.996)	0.249 (0.992)	0.008	0.007	0.003	—	—	0.002
	1/2	0.944 (0.931)	0.837 (0.942)	0.732 (0.977)	0.212 (0.991)	0.242 (0.992)	0.248 (0.988)	0.022	0.019	0.008	—	—	0.003
	2/3	0.911 (0.898)	0.813 (0.915)	0.724 (0.967)	0.211 (0.986)	0.240 (0.984)	0.246 (0.980)	0.042	0.036	0.016	—	—	0.004
60°	0	1.034 (1.000)	0.950 (1.000)	0.648 (1.000)	0.283 (1.000)	0.310 (1.000)	0.313 (1.000)	0.000	0.000	0.000	—	0.000	0.000
	1/3	0.998 (0.965)	0.920 (0.968)	0.637 (0.983)	0.281 (0.993)	0.307 (0.990)	0.311 (0.994)	0.012	0.011	0.006	—	0.000	0.002
	1/2	0.966 (0.934)	0.893 (0.940)	0.626 (0.966)	0.279 (0.986)	0.305 (0.984)	0.308 (0.984)	0.033	0.030	0.017	—	0.000	0.007
	2/3	0.935 (0.904)	0.866 (0.912)	0.616 (0.951)	0.276 (0.975)	0.301 (0.971)	0.306 (0.978)	0.061	0.056	0.032	—	0.001	0.019
90°	0	1.010 (1.000)	0.952 (1.000)	0.654 (1.000)	0.427 (1.000)	0.447 (1.000)	0.453 (1.000)	0.000	0.000	0.000	0.000	0.000	0.000
	1/3	0.982 (0.972)	0.926 (0.973)	0.641 (0.980)	0.422 (0.988)	0.442 (0.989)	0.445 (0.982)	0.028	0.027	0.020	0.001	0.001	0.001
	1/2	0.955 (0.946)	0.901 (0.946)	0.628 (0.960)	0.418 (0.979)	0.436 (0.935)	0.439 (0.969)	0.076	0.074	0.058	0.006	0.006	0.005
	2/3	0.923 (0.914)	0.872 (0.916)	0.613 (0.937)	0.414 (0.970)	0.431 (0.926)	0.433 (0.956)	0.152	0.147	0.118	0.016	0.015	0.013

Table 5c. F_{I,λ_1} and $F_{\mathrm{II},\lambda_2}$ for two diamond-shaped inclusions at the corner A under various loading conditions. (Plane strain state $\nu_1 = \nu_2 = 0.3$)

(c) In-plane shear

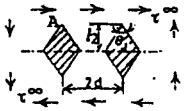

		F_{I,λ_1}						$F_{\mathrm{II},\lambda_2}(F_{\mathrm{II},\lambda_2}/F_{\mathrm{II},\lambda_2}\|_{l_2/d=0})$					
G_2/G_1		10^{-5}	10^{-2}	10^{-1}	10^{1}	10^{2}	10^{5}	10^{-5}	10^{-2}	10^{-1}	10^{1}	10^{2}	10^{5}
θ_A	l_2/d												
	0	0.000	0.000	0.000	0.000	0.000	0.000	1.154	1.126	1.026	—	—	−0.584
								(1.000)	(1.000)	(1.000)			(1.000)
	1/3	0.008	0.007	0.005	0.001	0.001	0.002	1.171	1.142	1.035	—	—	−0.609
30°								(1.015)	(1.014)	(1.009)			(1.043)
	1/2	0.023	0.021	0.015	0.001	0.002	0.006	1.184	1.154	1.042	—	—	−0.596
								(1.026)	(1.025)	(1.016)			(1.021)
	2/3	0.048	0.043	0.031	0.003	0.003	0.012	1.194	1.162	1.046	—	—	−0.579
								(1.035)	(1.032)	(1.019)			(0.991)
	0	0.000	0.000	0.000	0.000	0.000	0.000	1.599	1.586	1.507	—	−0.721	−0.651
								(1.000)	(1.000)	(1.000)		(1.000)	(1.000)
	1/3	0.012	0.011	0.007	0.002	0.002	0.004	1.629	1.613	1.526	—	−0.729	−0.628
60°								(1.019)	(1.017)	(1.013)		(1.011)	(0.965)
	1/2	0.038	0.035	0.022	0.005	0.006	0.010	1.650	1.634	1.540	—	−0.716	−0.607
								(1.032)	(1.030)	(1.022)		(0.993)	(0.932)
	2/3	0.080	0.073	0.045	0.009	0.011	0.018	1.662	1.646	1.547	—	−0.706	−0.585
								(1.039)	(1.038)	(1.027)		(0.979)	(0.899)
	0	0.000	0.000	0.000	0.000	0.000	0.000	4.279	4.318	4.723	−0.987	−0.769	−0.769
								(1.000)	(1.000)	(1.000)	(1.000)	(1.000)	(1.000)
	1/3	0.026	0.024	0.015	0.004	0.005	0.005	4.390	4.426	4.816	−0.972	−0.755	−0.755
90°								(1.026)	(1.025)	(1.020)	(0.985)	(0.982)	(0.982)
	1/2	0.083	0.078	0.047	0.010	0.013	0.013	4.455	4.490	4.868	−0.965	−0.748	−0.748
								(1.041)	(1.040)	(1.031)	(0.978)	(0.973)	(0.973)
	2/3	0.188	0.175	0.102	0.016	0.019	0.019	4.436	4.471	4.849	−0.968	−0.750	−0.750
								(1.037)	(1.035)	(1.027)	(0.981)	(0.975)	(0.975)

Table 7 and Table 8 show the accuracy of the extrapolated values when $N \to \infty$ by using the linear relationship between $F_{\mathrm{I},\lambda_1,k}$ (or $F_{\mathrm{II},\lambda_2,k}$) and $1/N$. In Table 7, $F_{\mathrm{I},\lambda_1,k}$ values at the corner C under uniaxial tension (x-direction), when $\theta_A = 30°$ and $G_2/G_1 = 10^{-1}$ are shown. In Table 8, $F_{\mathrm{II},\lambda_2,k}$ values at the corner C under in-plane shear, when $\theta_A = 30°$ and $G_2/G_1 = 10^{-1}$ are shown. Here, the values of ∞(2-4) are the extrapolated values from the results of $N = 2$ and $N = 4$. From these tables, the errors of the extrapolated values are within one percent even when $l_2/d = \frac{2}{3}$.

Table 6a. F_{I,λ_1} and F_{II,λ_2} for two diamond-shaped inclusions at the corner B and B' under various loading conditions. (Plane strain state $\nu_1 = \nu_2 = 0.3$). $F_{1B,\lambda_1} = F_{I,\lambda_1}$ at the corner B

(a) Uniaxial tension

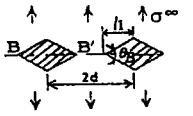

		$F_{1B,\lambda_1}(F_{1B,\lambda_1}/F_{I,\lambda_1}\|_{l_1/d=0})$						$F_{1B',\lambda_1}(F_{1B',\lambda_1}/F_{I,\lambda_1}\|_{l_1/d=0})$					
G_2/G_1		10^{-5}	10^{-2}	10^{-1}	10^{1}	10^{2}	10^{5}	10^{-5}	10^{-2}	10^{-1}	10^{1}	10^{2}	10^{5}
θ_B	l_1/d												
30°	0	1.042	0.909	0.747	−0.160	−0.174	−0.177	1.042	0.909	0.747	−0.160	−0.174	−0.177
		(1.000)	(1.000)	(1.000)	(1.000)	(1.000)	(1.000)	(1.000)	(1.000)	(1.000)	(1.000)	(1.000)	(1.000)
	1/3	1.057	0.921	0.754	−0.164	−0.178	−0.181	1.062	0.925	0.755	−0.165	−0.179	−0.184
		(1.014)	(1.013)	(1.009)	(1.025)	(1.023)	(1.023)	(1.019)	(1.018)	(1.011)	(1.031)	(1.029)	(1.040)
	1/2	1.072	0.932	0.757	−0.166	−0.180	−0.183	1.092	0.947	0.764	−0.169	−0.185	−0.193
		(1.029)	(1.025)	(1.013)	(1.038)	(1.034)	(1.034)	(1.048)	(1.042)	(1.023)	(1.056)	(1.063)	(1.090)
	2/3	1.096	0.948	0.761	−0.168	−0.184	−0.189	1.156	0.996	0.783	−0.179	−0.199	−0.204
		(1.052)	(1.043)	(1.019)	(1.050)	(1.057)	(1.068)	(1.109)	(1.096)	(1.048)	(1.119)	(1.144)	(1.153)
60°	0	1.148	1.054	0.717	−0.154	−0.173	−0.175	1.148	1.054	0.717	−0.154	−0.173	−0.175
		(1.000)	(1.000)	(1.000)	(1.000)	(1.000)	(1.000)	(1.000)	(1.000)	(1.000)	(1.000)	(1.000)	(1.000)
	1/3	1.160	1.065	0.721	−0.152	−0.172	−0.175	1.164	1.068	0.722	−0.154	−0.175	−0.178
		(1.010)	(1.010)	(1.006)	(0.987)	(0.994)	(1.000)	(1.014)	(1.013)	(1.007)	(1.000)	(1.012)	(1.017)
	1/2	1.174	1.076	0.725	−0.155	−0.176	−0.181	1.190	1.090	0.731	−0.162	−0.185	−0.187
		(1.023)	(1.021)	(1.011)	(1.006)	(1.017)	(1.034)	(1.037)	(1.034)	(1.020)	(1.052)	(1.069)	(1.069)
	2/3	1.197	1.095	0.730	−0.159	−0.181	−0.186	1.252	1.143	0.753	−0.178	−0.206	−0.208
		(1.043)	(1.039)	(1.018)	(1.032)	(1.046)	(1.063)	(1.091)	(1.084)	(1.050)	(1.156)	(1.191)	(1.189)
90°	0	1.293	1.223	0.858	−0.131	−0.148	−0.152	1.293	1.223	0.858	−0.131	−0.148	−0.152
		(1.000)	(1.000)	(1.000)	(1.000)	(1.000)	(1.000)	(1.000)	(1.000)	(1.000)	(1.000)	(1.000)	(1.000)
	1/3	1.300	1.229	0.860	−0.144	−0.158	−0.161	1.299	1.228	0.860	−0.149	−0.165	−0.170
		(1.005)	(1.005)	(1.002)	(1.099)	(1.068)	(1.059)	(1.005)	(1.004)	(1.002)	(1.137)	(1.115)	(1.118)
	1/2	1.313	1.240	0.865	−0.149	−0.163	−0.168	1.317	1.244	0.867	−0.167	−0.188	−0.189
		(1.015)	(1.014)	(1.008)	(1.137)	(1.101)	(1.105)	(1.019)	(1.017)	(1.010)	(1.275)	(1.270)	(1.243)
	2/3	1.336	1.262	0.873	−0.154	−0.169	−0.175	1.374	1.296	0.893	−0.201	−0.231	−0.221
		(1.033)	(1.032)	(1.017)	(1.176)	(1.142)	(1.151)	(1.063)	(1.060)	(1.041)	(1.534)	(1.561)	(1.454)

Table 6b. F_{I,λ_1} and $F_{\mathrm{II},\lambda_2}$ for two diamond-shaped inclusions at the corner B and B' under various loading conditions. (Plane strain state $\nu_1 = \nu_2 = 0.3$). $F_{IB,\lambda_1} = F_{\mathrm{I},\lambda_1}$ at the corner B

(b) Biaxial tension

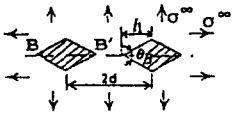

		$F_{IB,\lambda_1}(F_{IB,\lambda_1}/F_{\mathrm{I},\lambda_1}\|_{l_1/d=0})$						$F_{IB',\lambda_1}(F_{IB',\lambda_1}/F_{\mathrm{I},\lambda_1}\|_{l_1/d=0})$					
G_2/G_1		10^{-5}	10^{-2}	10^{-1}	10^{1}	10^{2}	10^{5}	10^{-5}	10^{-2}	10^{-1}	10^{1}	10^{2}	10^{5}
θ_B	l_1/d												
	0	1.014	0.889	0.749	0.214	0.244	0.251	1.014	0.889	0.749	0.214	0.244	0.251
		(1.000)	(1.000)	(1.000)	(1.000)	(1.000)	(1.000)	(1.000)	(1.000)	(1.000)	(1.000)	(1.000)	(1.000)
	1/3	1.031	0.900	0.750	0.215	0.245	0.251	1.036	0.904	0.752	0.215	0.247	0.254
30°		(1.017)	(1.012)	(1.001)	(1.005)	(1.004)	(1.000)	(1.022)	(1.017)	(1.004)	(1.005)	(1.012)	(1.012)
	1/2	1.046	0.912	0.754	0.216	0.247	0.253	1.067	0.928	0.763	0.219	0.254	0.266
		(1.032)	(1.026)	(1.007)	(1.009)	(1.012)	(1.008)	(1.052)	(1.044)	(1.019)	(1.023)	(1.041)	(1.060)
	2/3	1.071	0.929	0.758	0.218	0.254	0.256	1.133	0.979	0.783	0.230	0.273	0.295
		(1.056)	(1.045)	(1.012)	(1.019)	(1.041)	(1.020)	(1.117)	(1.101)	(1.045)	(1.075)	(1.119)	(1.175)
	0	1.034	0.950	0.648	0.283	0.310	0.313	1.034	0.950	0.648	0.283	0.310	0.313
		(1.000)	(1.000)	(1.000)	(1.000)	(1.000)	(1.000)	(1.000)	(1.000)	(1.000)	(1.000)	(1.000)	(1.000)
	1/3	1.051	0.964	0.653	0.283	0.312	0.313	1.057	0.970	0.656	0.283	0.312	0.315
60°		(1.016)	(1.015)	(1.008)	(1.000)	(1.006)	(1.000)	(1.022)	(1.021)	(1.012)	(1.000)	(1.006)	(1.006)
	1/2	1.069	0.980	0.659	0.284	0.313	0.317	1.093	1.001	0.670	0.291	0.323	0.327
		(1.034)	(1.032)	(1.017)	(1.004)	(1.010)	(1.013)	(1.057)	(1.054)	(1.034)	(1.028)	(1.042)	(1.045)
	2/3	1.097	1.003	0.667	0.288	0.319	0.323	1.168	1.066	0.700	0.311	0.348	0.356
		(1.061)	(1.056)	(1.029)	(1.018)	(1.029)	(1.032)	(1.130)	(1.122)	(1.080)	(1.099)	(1.123)	(1.137)
	0	1.010	0.952	0.654	0.427	0.447	0.453	1.010	0.952	0.654	0.427	0.447	0.453
		(1.000)	(1.000)	(1.000)	(1.000)	(1.000)	(1.000)	(1.000)	(1.000)	(1.000)	(1.000)	(1.000)	(1.000)
	1/3	1.038	0.977	0.667	0.430	0.452	0.454	1.052	0.990	0.673	0.434	0.456	0.459
90°		(1.028)	(1.026)	(1.020)	(1.007)	(1.011)	(1.002)	(1.042)	(1.040)	(1.029)	(1.016)	(1.020)	(1.013)
	1/2	1.065	1.002	0.678	0.434	0.456	0.458	1.111	1.045	0.702	0.447	0.473	0.477
		(1.054)	(1.053)	(1.037)	(1.016)	(1.020)	(1.011)	(1.100)	(1.098)	(1.073)	(1.047)	(1.058)	(1.053)
	2/3	1.101	1.034	0.693	0.439	0.462	0.464	1.210	1.135	0.751	0.479	0.514	0.523
		(1.090)	(1.086)	(1.060)	(1.028)	(1.034)	(1.024)	(1.198)	(1.192)	(1.148)	(1.122)	(1.150)	(1.155)

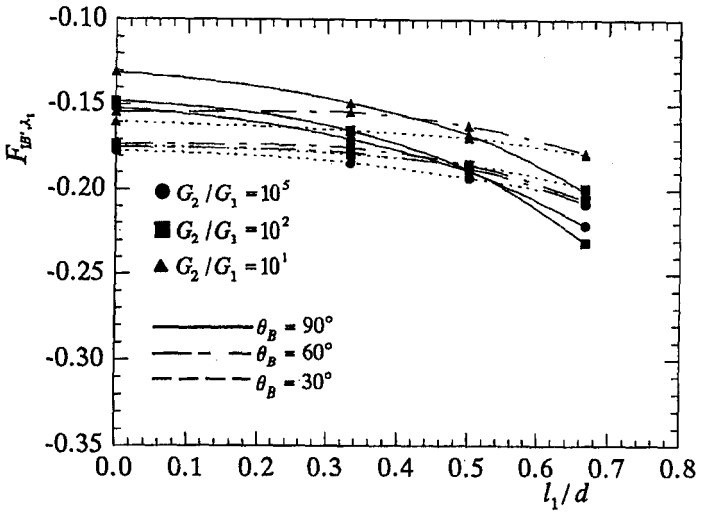

Figure 4. Interaction of F_{I,λ_1} for two diamond-shaped inclusions at the corner B' under uniaxial tension (y-direction). ($G_2/G_1 > 1$, plane strain state $\nu_1 = \nu_2 = 0.3$).

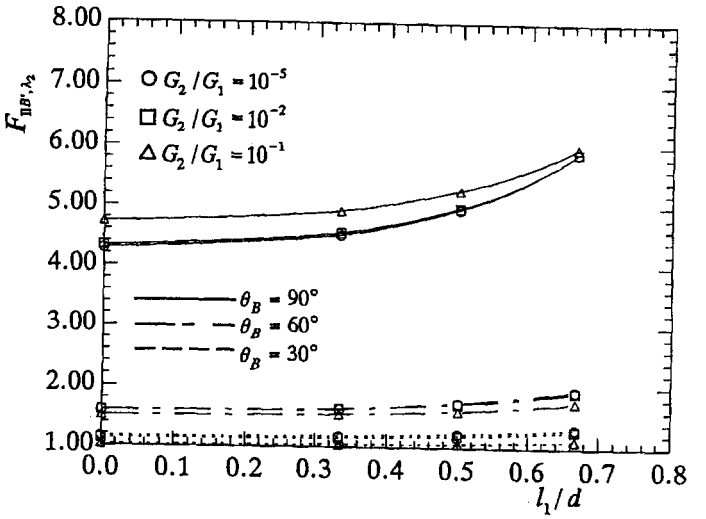

Figure 5. Interaction of $F_{\mathrm{II},\lambda_2}$ for two diamond-shaped inclusions at the corner B' under in-plane shear. ($G_2/G_1 < 1$, plane strain state $\nu_1 = \nu_2 = 0.3$).

Table 9 and Table 10 show $F_{\mathrm{I},\lambda_1,k}$ or $F_{\mathrm{II},\lambda_2,k}$ when $N = 2, 4, 5, \infty$. On the other hand, Figure 7 and Figure 8 show the relation between $F_{\mathrm{I},\lambda_1,k}$ or $F_{\mathrm{II},\lambda_2,k}$ when $N = 2, 4, 5, \infty$. Those results are plotted in Figure 7 and Figure 8. In those tables and figures, the difference among the results when $N = 2, 4, 5, \infty$ increases with increasing l_2/d.

Tables 11 and 12 show the extrapolated values when $N \to \infty$ by using the linear relationship between $F_{\mathrm{I},\lambda_1,k}$ (or $F_{\mathrm{II},\lambda_2,k}$) and $1/N$. Here, the value in parenthesis shows the ratio to the values of a single inclusion. The results for the corner A, C when $\theta_A \leq 90°$ are shown in Table 11 and the ones for the corner B, B', D when $\theta_B \leq 90°$ are shown in Table 12 (see Figure 1). Figures 9 and 10 show the relation between the stress intensity factors and l_1/d at

Table 6c. F_{I,λ_1} and $F_{\mathrm{II},\lambda_2}$ for two diamond-shaped inclusions at the corner B and B' under various loading conditions. (Plane strain state $\nu_1 = \nu_2 = 0.3$). $F_{\mathrm{I}B,\lambda_1} = F_{\mathrm{I},\lambda_1}$ at the corner B

(c) In-plane shear

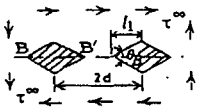

		$F_{\mathrm{II}B,\lambda_2}(F_{\mathrm{II}B,\lambda_2}/F_{\mathrm{II},\lambda_2}\|_{l_1/d=0})$						$F_{\mathrm{II}B',\lambda_2}(F_{\mathrm{II}B',\lambda_2}/F_{\mathrm{II},\lambda_2}\|_{l_1/d=0})$					
G_2/G_1		10^{-5}	10^{-2}	10^{-1}	10^{1}	10^{2}	10^{5}	10^{-5}	10^{-2}	10^{-1}	10^{1}	10^{2}	10^{5}
θ_B	l_1/d												
	0	1.154	1.126	1.026	—	—	−0.584	1.154	1.126	1.026	—	—	−0.584
		(1.000)	(1.000)	(1.000)			(1.000)	(1.000)	(1.000)	(1.000)			(1.000)
	1/3	1.172	1.142	1.035	—	—	−0.570	1.181	1.150	1.041	—	—	−0.611
30°		(1.016)	(1.014)	(1.009)			(0.976)	(1.023)	(1.021)	(1.015)			(1.046)
	1/2	1.191	1.159	1.045	—	—	−0.567	1.226	1.192	1.067	—	—	−0.655
		(1.032)	(1.029)	(1.019)			(0.971)	(1.062)	(1.059)	(1.040)			(1.122)
	2/3	1.218	1.183	1.058	—	—	−0.567	1.325	1.284	1.123	—	—	−0.694
		(1.055)	(1.051)	(1.031)			(0.971)	(1.148)	(1.140)	(1.095)			(1.188)
	0	1.599	1.586	1.507	—	−0.721	−0.651	1.599	1.586	1.507	—	−0.721	−0.651
		(1.000)	(1.000)	(1.000)		(1.000)	(1.000)	(1.000)	(1.000)	(1.000)	—	(1.000)	(1.000)
	1/3	1.626	1.612	1.525	—	−0.717	−0.643	1.620	1.635	1.542	—	−0.742	−0.685
60°		(1.017)	(1.016)	(1.012)		(0.994)	(0.988)	(1.013)	(1.031)	(1.023)		(1.029)	(1.052)
	1/2	1.654	1.638	1.544	—	−0.709	−0.639	1.743	1.724	1.606	—	−0.759	−0.730
		(1.034)	(1.033)	(1.025)		(0.983)	(0.982)	(1.090)	(1.087)	(1.066)		(1.053)	(1.121)
	2/3	1.689	1.671	1.567	—	−0.699	−0.636	1.949	1.921	1.745	—	−0.804	−0.824
		(1.056)	(1.054)	(1.040)		(0.969)	(0.977)	(1.219)	(1.211)	(1.158)		(1.115)	(1.266)
	0	4.279	4.318	4.723	−0.987	−0.769	−0.769	4.279	4.318	4.723	−0.987	−0.769	−0.769
		(1.000)	(1.000)	(1.000)	(1.000)	(1.000)	(1.000)	(1.000)	(1.000)	(1.000)	(1.000)	(1.000)	(1.000)
	1/3	4.365	4.403	4.799	−0.970	−0.753	−0.753	4.507	4.541	4.911	−0.967	−0.752	−0.752
90°		(1.020)	(1.020)	(1.016)	(0.983)	(0.979)	(0.979)	(1.053)	(1.052)	(1.040)	(0.980)	(0.978)	(0.978)
	1/2	4.434	4.471	4.864	−0.954	−0.737	−0.737	4.944	4.967	5.260	−0.946	−0.737	−0.737
		(1.036)	(1.035)	(1.030)	(0.967)	(0.958)	(0.958)	(1.156)	(1.150)	(1.114)	(0.958)	(0.958)	(0.958)
	2/3	4.504	4.541	4.931	−0.935	−0.717	−0.717	5.888	5.881	5.968	−0.931	−0.736	−0.736
		(1.053)	(1.052)	(1.044)	(0.947)	(0.932)	(0.932)	(1.376)	(1.362)	(1.264)	(0.943)	(0.957)	(0.957)

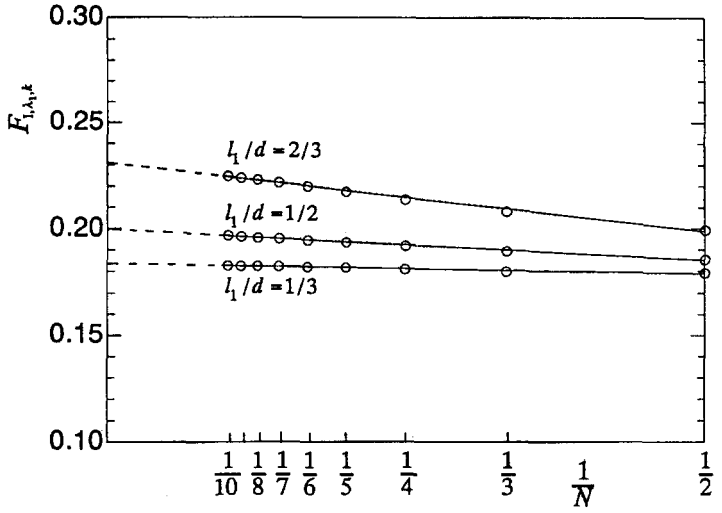

Figure 6. $F_{I,\lambda_1,k} - 1/N$ relations. ($\theta_B = 30°, G_2/G_1 = 10^2, \sigma_y^\infty = \sigma^\infty, \sigma_x^\infty = \tau_{xy}^\infty = 0$, plane strain state $\nu_1 = \nu_2 = 0.3$)

Table 7. The extrapolated values of $F_{I,\lambda_1,k}$ at the corner C. ($\theta_A = 30°, G_2/G_1 = 10^{-1}, \sigma_x^\infty = \sigma^\infty, \sigma_y^\infty = \tau_{xy}^\infty = 0$, plane strain state $\nu_1 = \nu_2 = 0.3$)

N	l_2/d	$F_{I,\lambda_1,k}(\lambda_1 = 0.7851341)$		
		$\frac{1}{3}$	$\frac{1}{2}$	$\frac{2}{3}$
2		0.7352	0.7248	0.7151
4		0.7211	0.6976	0.6758
5		0.7182	0.6926	0.6671
∞(2-4)		0.707	0.670	0.637
∞(4-5)		0.707	0.673	0.632

Table 8. The extrapolated values of $F_{II,\lambda_2,k}$ at the corner C. ($\theta_A = 30°, G_2/G_1 = 10^{-1}, \tau_{xy}^\infty = \tau^\infty, \sigma_x^\infty = \tau_y^\infty = 0$, plane strain state $\nu_1 = \nu_2 = 0.3$)

N	l_2/d	$F_{II,\lambda_2,k}(\lambda_2 = 0.7239281)$		
		$\frac{1}{3}$	$\frac{1}{2}$	$\frac{2}{3}$
7		1.0513	1.0742	1.0947
8		1.0520	1.0758	1.0977
9		1.0527	1.0775	1.1007
∞(7-8)		1.057	1.087	1.119
∞(8-9)		1.058	1.091	1.125

Table 9. $F_{\mathrm{I},\lambda_1,k}$ at the corner A when $N = 2, N = 4, N = 5$ and $N \to \infty$. ($\theta_A = 90°, G_2/G_1 > 1, \sigma_x^\infty = \sigma_y^\infty = \sigma^\infty, \tau_{xy}^\infty = 0$, plane strain state $\nu_1 = \nu_2 = 0.3$)

G_2/G_1	l_2/d	$F_{\mathrm{I},\lambda_1,k}(\theta_A = 90°)$			
		N 2	4	5	∞
10^5	0	0.453	0.453	0.453	0.453
	$\frac{1}{3}$	0.445	0.444	0.443	0.442
	$\frac{1}{2}$	0.439	0.435	0.434	0.431
	$\frac{2}{3}$	0.433	0.425	0.424	0.418
10^2	0	0.447	0.447	0.447	0.447
	$\frac{1}{3}$	0.442	0.440	0.440	0.439
	$\frac{1}{2}$	0.436	0.432	0.431	0.428
	$\frac{2}{3}$	0.431	0.423	0.421	0.414
10^1	0	0.427	0.427	0.427	0.427
	$\frac{1}{3}$	0.422	0.421	0.421	0.420
	$\frac{1}{2}$	0.418	0.414	0.414	0.411
	$\frac{2}{3}$	0.414	0.407	0.406	0.401

Table 10. $F_{\mathrm{II},\lambda_2,k}$ at the corner C when $N = 2, N = 4, N = 5$ and $N \to \infty$. ($\theta_A = 90°, G_2/G_1 < 1, \tau_{xy}^\infty = \tau^\infty, \sigma_x^\infty = \sigma_y^\infty = 0$, plane strain state $\nu_1 = \nu_2 = 0.3$)

G_2/G_1	l_2/d	$F_{\mathrm{II},\lambda_2,k}(\theta_A = 90°)$			
		N 2	4	5	∞
10^{-5}	0	4.279	4.279	4.279	4.279
	$\frac{1}{3}$	4.390	4.540	4.579	4.703
	$\frac{1}{2}$	4.455	4.728	4.814	5.156
	$\frac{2}{3}$	4.436	4.758	4.917	5.717
10^{-2}	0	4.318	4.318	4.318	4.318
	$\frac{1}{3}$	4.426	4.574	4.611	4.734
	$\frac{1}{2}$	4.490	4.756	4.843	5.188
	$\frac{2}{3}$	4.471	4.785	4.937	5.720
10^{-1}	0	4.723	4.723	4.723	4.723
	$\frac{1}{3}$	4.816	4.942	4.973	5.078
	$\frac{1}{2}$	4.868	5.089	5.160	5.437
	$\frac{2}{3}$	4.849	5.101	5.222	5.765

the corner D. As shown in Figure 9 for $\theta_B \leq 90°$ and $G_2/G_1 > 1$ under uniaxial tension (y-direction), the interaction appears largely and $F_{\mathrm{I},\lambda_1,k}$ is about twice as large as that of a single inclusion at $l_1/d = \frac{2}{3}$ and $\theta_B = 90°$, even though the absolute value is small. On the other hand, as shown in Figure 10 for $\theta_B \leq 90°$ and $G_2/G_1 < 1$ under in-plane shear, the interaction appears also largely by about eighty percent when $l_1/d = \frac{2}{3}$ and $\theta_B = 90°$, and the absolute value is also large in this case.

Table 11a. $F_{IA,\infty}$, $F_{IIA,\infty}$ and $F_{IC,\infty}(F_{IIC,\infty})$ for a row of diamond-shaped inclusions (number of inclusion; $N \to \infty$) at the corner A and C under various loading conditions. (Plane strain state $\nu_1 = \nu_2 = 0.3$). $F_{IA,\infty} = F_{I,\lambda_1,k}$ at the corner A when $N \to \infty$.

(a) Uniaxial tension

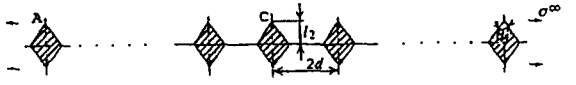

		$F_{IA,\infty}(F_{IA,\infty}/F_{I,\lambda_1}\|_{l_2/d=0})$						$F_{IIA,\infty}$						$F_{IC,\infty}(F_{IC,\infty}/F_{I,\lambda_1}\|_{l_2/d=0})$					
G_2/G_1		10^{-5}	10^{-2}	10^{-1}	10^{1}	10^{2}	10^{5}	10^{-5}	10^{-2}	10^{-1}	10^{1}	10^{2}	10^{5}	10^{-5}	10^{-2}	10^{-1}	10^{1}	10^{2}	10^{5}
θ_A	l_2/d																		
30°	0	1.042	0.909	0.747	−0.160	−0.174	−0.177	0.000	0.000	0.000	—	—	0.000	1.042	0.909	0.747	−0.160	−0.174	−0.177
		(1.000)	(1.000)	(1.000)	(1.000)	(1.000)	(1.000)							(1.000)	(1.000)	(1.000)	(1.000)	(1.000)	(1.000)
	$\frac{1}{3}$	0.975	0.856	0.727	−0.163	−0.175	−0.180	0.013	0.010	0.004	—	—	0.006	0.893	0.804	0.707	−0.163	−0.178	−0.182
		(0.936)	(0.942)	(0.973)	(1.019)	(1.006)	(1.017)							(0.857)	(0.884)	(0.946)	(1.019)	(1.023)	(1.028)
	$\frac{1}{2}$	0.918	0.811	0.708	−0.163	−0.176	−0.181	0.030	0.026	0.013	—	—	0.012	0.770	0.717	0.673	−0.164	−0.179	−0.190
		(0.881)	(0.892)	(0.948)	(1.019)	(1.011)	(1.023)							(0.739)	(0.789)	(0.901)	(1.025)	(1.029)	(1.073)
	$\frac{2}{3}$	0.867	0.770	0.690	−0.164	−0.178	−0.185	0.052	0.046	0.026	—	—	0.019	0.655	0.638	0.636	−0.166	−0.181	−0.192
		(0.832)	(0.847)	(0.924)	(1.025)	(1.023)	(1.045)							(0.629)	(0.702)	(0.851)	(1.038)	(1.040)	(1.085)
60°	0	1.148	1.054	0.717	−0.154	−0.173	−0.175	0.000	0.000	0.000	—	0.000	0.000	1.148	1.054	0.717	−0.154	−0.173	−0.175
		(1.000)	(1.000)	(1.000)	(1.000)	(1.000)	(1.000)							(1.000)	(1.000)	(1.000)	(1.000)	(1.000)	(1.000)
	$\frac{1}{3}$	1.066	0.980	0.686	−0.159	−0.179	−0.179	0.022	0.021	0.014	—	0.004	0.002	0.968	0.911	0.651	−0.163	−0.182	−0.184
		(0.929)	(0.930)	(0.957)	(1.032)	(1.035)	(1.023)							(0.843)	(0.864)	(0.908)	(1.058)	(1.052)	(1.051)
	$\frac{1}{2}$	1.000	0.923	0.658	−0.161	−0.184	−0.186	0.055	0.053	0.036	—	0.011	0.004	0.823	0.793	0.599	−0.166	−0.190	−0.195
		(0.871)	(0.876)	(0.918)	(1.045)	(1.064)	(1.063)							(0.717)	(0.752)	(0.835)	(1.078)	(1.098)	(1.114)
	$\frac{2}{3}$	0.943	0.872	0.633	−0.165	−0.187	−0.191	0.094	0.090	0.064	—	0.024	0.008	0.756	0.702	0.547	−0.169	−0.194	−0.206
		(0.821)	(0.827)	(0.883)	(1.071)	(1.081)	(1.091)							(0.659)	(0.666)	(0.763)	(1.097)	(1.121)	(1.177)
90°	0	1.293	1.223	0.858	−0.131	−0.148	−0.152	0.000	0.000	0.000	0.000	0.000	0.000	1.293	1.223	0.858	−0.131	−0.148	−0.152
		(1.000)	(1.000)	(1.000)	(1.000)	(1.000)	(1.000)							(1.000)	(1.000)	(1.000)	(1.000)	(1.000)	(1.000)
	$\frac{1}{3}$	1.192	1.128	0.808	−0.149	−0.163	−0.163	0.081	0.079	0.063	0.008	0.008	0.007	1.072	1.033	0.757	−0.153	−0.169	−0.169
		(0.922)	(0.922)	(0.942)	(1.137)	(1.101)	(1.072)							(0.829)	(0.845)	(0.882)	(1.168)	(1.142)	(1.112)
	$\frac{1}{2}$	1.113	1.054	0.768	−0.157	−0.171	−0.172	0.197	0.195	0.166	0.028	0.028	0.025	0.898	0.893	0.677	−0.164	−0.184	−0.184
		(0.861)	(0.862)	(0.895)	(1.198)	(1.155)	(1.132)							(0.695)	(0.730)	(0.789)	(1.252)	(1.243)	(1.211)
	$\frac{2}{3}$	1.051	0.997	0.733	−0.158	−0.178	−0.179	0.321	0.317	0.286	0.069	0.066	0.052	0.835	0.786	0.607	−0.175	−0.188	−0.201
		(0.813)	(0.815)	(0.854)	(1.206)	(1.203)	(1.178)							(0.646)	(0.643)	(0.707)	(1.336)	(1.270)	(1.322)

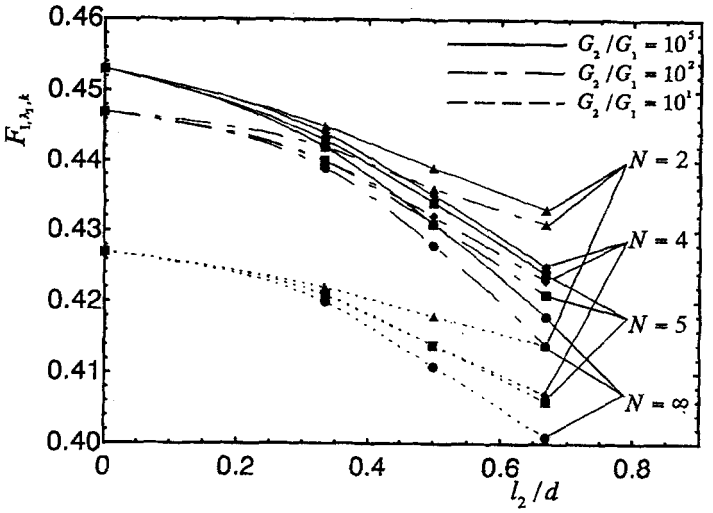

Figure 7. Interaction of $F_{I,\lambda_1,k}$ at the corner A when $N = 2, N = 4, N = 5$ and $N \to \infty$. ($\theta_A = 90°, G_2/G_1 > 1, \sigma_x^\infty = \sigma_y^\infty = \sigma^\infty, \tau_{xy}^\infty = 0$, plane strain state $\nu_1 = \nu_2 = 0.3$).

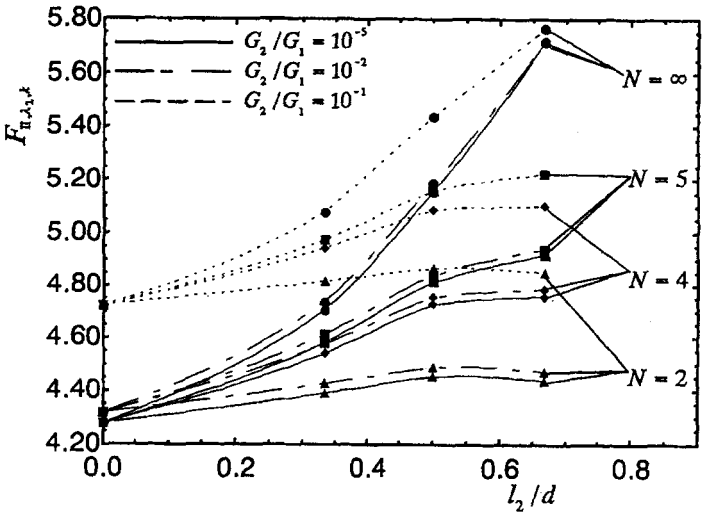

Figure 8. Interaction of $F_{II,\lambda_2,k}$ at the corner C when $N = 2, N = 4, N = 5$ and $N \to \infty$. ($\theta_A = 90°, G_2/G_1 < 1, \tau_{xy}^\infty = \tau^\infty, \sigma_x^\infty = \sigma_y^\infty = 0$, plane strain state $\nu_1 = \nu_2 = 0.3$).

Figure 11 shows the values of the stress intensity factors ($F_{I,\lambda_1,k}$) of each diamond-shaped inclusion when $N = 2 \sim 10, \theta_B = 30°, l_1/d = \frac{2}{3}$ and $G_2/G_1 = 10^1$ under biaxial tension. The vertical axis of the figure indicates the ratio of $F_{I,\lambda_1,k}$ to $F_{I,\lambda_1}|_{l_1/d=0}$. In Figure 11, the maximum stress intensity factors occur at the central inclusions, the minimum stress intensity factors occur at the outermost inclusions. In all cases, the maximum stress intensity factors appear at either the central inclusions or the outermost inclusions. The maximum stress intensity factors are shown in the thick lines of Tables 11 and 12. In Table 11(a) for $\theta_A \leq 90°$, under uniaxial tension (x-direction), the maximum stress intensity factors occur at the outermost diamond-shaped inclusions when $G_2/G_1 < 1$ and at the central inclusions when $G_2/G_1 > 1$. Under biaxial tension as shown in Table 11(b), the maximum values always

Table 11b. $F_{IA,\infty}$, $F_{IIA,\infty}$ and $F_{IC,\infty}(F_{IIC,\infty})$ for a row of diamond-shaped inclusions (number of inclusion; $N \to \infty$) at the corner A and C under various loading conditions. (Plane strain state $\nu_1 = \nu_2 = 0.3$). $F_{IA,\infty} = F_{I,\lambda_1,k}$ at the corner A when $N \to \infty$.

(b) Biaxial tension

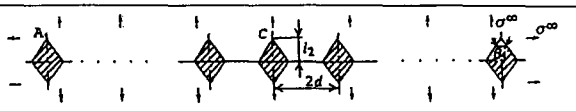

		$F_{IA,\infty}(F_{IA,\infty}/F_{I,\lambda_1}\|_{l_2/d=0})$						$F_{IIA,\infty}$						$F_{IC,\infty}(F_{IC,\infty}/F_{I,\lambda_1}\|_{l_2/d=0})$					
G_2/G_1		10^{-5}	10^{-2}	10^{-1}	10^{1}	10^{2}	10^{5}	10^{-5}	10^{-2}	10^{-1}	10^{1}	10^{2}	10^{5}	10^{-5}	10^{-2}	10^{-1}	10^{1}	10^{2}	10^{5}
θ_A	l_2/d																		
30°	0	1.014	0.889	0.749	0.214	0.244	0.251	0.000	0.000	0.000	—	—	0.000	1.014	0.889	0.749	0.214	0.244	0.251
		(1.000)	(1.000)	(1.000)	(1.000)	(1.000)	(1.000)							(1.000)	(1.000)	(1.000)	(1.000)	(1.000)	(1.000)
	$\frac{1}{3}$	0.956	0.845	0.734	0.213	0.243	0.248	0.010	0.009	0.003	—	—	0.015	0.887	0.799	0.719	0.212	0.241	0.245
		(0.943)	(0.951)	(0.980)	(0.995)	(0.996)	(0.988)							(0.875)	(0.899)	(0.960)	(0.991)	(0.988)	(0.976)
	$\frac{1}{2}$	0.907	0.807	0.718	0.212	0.240	0.248	0.026	0.023	0.010	—	—	0.021	0.780	0.721	0.691	0.210	0.236	0.234
		(0.894)	(0.908)	(0.959)	(0.991)	(0.984)	(0.988)							(0.769)	(0.811)	(0.923)	(0.981)	(0.967)	(0.932)
	$\frac{2}{3}$	0.862	0.770	0.704	0.209	0.237	0.244	0.044	0.040	0.020	—	—	0.029	0.679	0.664	0.658	0.202	0.230	0.216
		(0.850)	(0.866)	(0.940)	(0.977)	(0.971)	(0.972)							(0.670)	(0.747)	(0.879)	(0.944)	(0.943)	(0.861)
60°	0	1.034	0.950	0.648	0.283	0.310	0.313	0.000	0.000	0.000	—	0.000	0.000	1.034	0.950	0.648	0.283	0.310	0.313
		(1.000)	(1.000)	(1.000)	(1.000)	(1.000)	(1.000)							(1.000)	(1.000)	(1.000)	(1.000)	(1.000)	(1.000)
	$\frac{1}{3}$	0.979	0.902	0.629	0.278	0.305	0.308	0.014	0.013	0.008	—	0.000	0.006	0.912	0.854	0.608	0.273	0.299	0.302
		(0.947)	(0.949)	(0.971)	(0.982)	(0.984)	(0.984)							(0.882)	(0.899)	(0.938)	(0.965)	(0.965)	(0.965)
	$\frac{1}{2}$	0.934	0.862	0.613	0.274	0.300	0.302	0.037	0.036	0.021	—	0.000	0.007	0.810	0.777	0.576	0.267	0.293	0.294
		(0.903)	(0.907)	(0.946)	(0.968)	(0.968)	(0.965)							(0.783)	(0.818)	(0.889)	(0.943)	(0.945)	(0.939)
	$\frac{2}{3}$	0.893	0.826	0.599	0.269	0.293	0.293	0.063	0.060	0.038	—	0.003	0.014	0.715	0.708	0.543	0.256	0.279	0.281
		(0.864)	(0.869)	(0.924)	(0.951)	(0.945)	(0.936)							(0.691)	(0.745)	(0.893)	(0.905)	(0.900)	(0.898)
90°	0	1.010	0.952	0.654	0.427	0.447	0.453	0.000	0.000	0.000	0.000	0.000	0.000	1.010	0.952	0.654	0.427	0.447	0.453
		(1.000)	(1.000)	(1.000)	(1.000)	(1.000)	(1.000)							(1.000)	(1.000)	(1.000)	(1.000)	(1.000)	(1.000)
	$\frac{1}{3}$	0.968	0.911	0.633	0.420	0.439	0.442	0.032	0.031	0.025	0.003	0.003	0.001	0.912	0.870	0.611	0.412	0.426	0.434
		(0.958)	(0.957)	(0.968)	(0.984)	(0.982)	(0.976)							(0.903)	(0.914)	(0.934)	(0.965)	(0.408)	(0.958)
	$\frac{1}{2}$	0.935	0.881	0.614	0.411	0.428	0.431	0.076	0.074	0.063	0.010	0.008	0.005	0.833	0.811	0.571	0.397	0.408	0.410
		(0.926)	(0.925)	(0.939)	(0.963)	(0.957)	(0.951)							(0.825)	(0.852)	(0.873)	(0.930)	(0.913)	(0.905)
	$\frac{2}{3}$	0.907	0.854	0.596	0.401	0.414	0.418	0.133	0.147	0.118	0.026	0.025	0.013	0.812	0.760	0.526	0.376	0.384	0.385
		(0.898)	(0.897)	(0.911)	(0.939)	(0.926)	(0.923)							(0.804)	(0.798)	(0.804)	(0.881)	(0.859)	(0.850)

Table 11c. $F_{\mathrm{I}A,\infty}$, $F_{\mathrm{II}A,\infty}$ and $F_{\mathrm{I}C,\infty}(F_{\mathrm{II}C,\infty})$ for a row of diamond-shaped inclusions (number of inclusion; $N \to \infty$) at the corner A and C under various loading conditions. (Plane strain state $\nu_1 = \nu_2 = 0.3$). $F_{\mathrm{I}A,\infty} = F_{\mathrm{I},\lambda_1,k}$ at the corner A when $N \to \infty$.

(c) In-plane shear

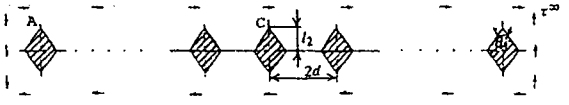

		$F_{\mathrm{I}A,\infty}$						$F_{\mathrm{II}A,\infty}(F_{\mathrm{II}A,\infty}/F_{\mathrm{II},\lambda_2}\|_{l_2/d=0})$						$F_{\mathrm{II}C,\infty}(F_{\mathrm{II}C,\infty}/F_{\mathrm{II},\lambda_2}\|_{l_2/d=0})$					
G_2/G_1		10^{-5}	10^{-2}	10^{-1}	10^{1}	10^{2}	10^{5}	10^{-5}	10^{-2}	10^{-1}	10^{1}	10^{2}	10^{5}	10^{-5}	10^{-2}	10^{-1}	10^{1}	10^{2}	10^{5}
θ_A	l_2/d																		
30°	0	0.000	0.000	0.000	0.000	0.000	0.000	1.154	1.126	1.026	—	—	−0.584	1.154	1.126	1.026	—	—	−0.584
								(1.000)	(1.000)	(1.000)			(1.000)	(1.000)	(1.000)	(1.000)			(1.000)
	$\frac{1}{3}$	0.013	0.013	0.007	0.001	0.001	0.002	1.183	1.152	1.043	—	—	−0.715	1.212	1.179	1.058	—	—	−0.635
								(1.025)	(1.023)	(1.017)			(1.224)	(1.050)	(1.047)	(1.031)			(1.087)
	$\frac{1}{2}$	0.032	0.027	0.023	0.003	0.002	0.006	1.214	1.179	1.059	—	—	−0.659	1.273	1.237	1.090	—	—	−0.610
								(1.052)	(1.047)	(1.032)			(1.128)	(1.103)	(1.099)	(1.062)			(1.045)
	$\frac{2}{3}$	0.070	0.062	0.041	0.003	0.005	0.013	1.250	1.214	1.077	—	—	−0.598	1.343	1.300	1.123	—	—	−0.564
								(1.083)	(1.078)	(1.050)			(1.024)	(1.164)	(1.155)	(1.095)			(0.966)
60°	0	0.000	0.000	0.000	0.000	0.000	0.000	1.599	1.586	1.507	—	−0.721	−0.651	1.599	1.586	1.507	—	−0.721	−0.651
								(1.000)	(1.000)	(1.000)		(1.000)	(1.000)	(1.000)	(1.000)	(1.000)		(1.000)	(1.000)
	$\frac{1}{3}$	0.018	0.017	0.011	0.002	0.002	0.004	1.653	1.636	1.545	—	−0.803	−0.770	1.705	1.688	1.579	—	−0.759	−0.686
								(1.034)	(1.032)	(1.025)		(1.114)	(1.183)	(1.066)	(1.064)	(1.048)		(1.053)	(1.054)
	$\frac{1}{2}$	0.056	0.049	0.028	0.007	0.008	0.011	1.709	1.691	1.575	—	−0.762	−0.699	1.815	1.795	1.653	—	−0.740	−0.657
								(1.069)	(1.066)	(1.045)		(1.057)	(1.074)	(1.135)	(1.132)	(1.097)		(1.026)	(1.009)
	$\frac{2}{3}$	0.126	0.103	0.064	0.013	0.015	0.020	1.771	1.747	1.614	—	−0.728	−0.629	1.941	1.918	1.729	—	−0.724	−0.625
								(1.108)	(1.102)	(1.071)		(1.010)	(0.966)	(1.214)	(1.209)	(1.147)		(1.004)	(0.960)
90°	0	0.000	0.000	0.000	0.000	0.000	0.000	4.279	4.318	4.723	−0.987	−0.769	−0.769	4.279	4.318	4.723	−0.987	−0.769	−0.769
								(1.000)	(1.000)	(1.000)	(1.000)	(1.000)	(1.000)	(1.000)	(1.000)	(1.000)	(1.000)	(1.000)	(1.000)
	$\frac{1}{3}$	0.038	0.036	0.021	0.006	0.007	0.007	4.496	4.530	4.906	−0.962	−0.745	−0.745	4.703	4.734	5.078	−0.939	−0.721	−0.721
								(1.051)	(1.049)	(1.039)	(0.975)	(0.969)	(0.969)	(1.099)	(1.096)	(1.075)	(0.951)	(1.938)	(0.938)
	$\frac{1}{2}$	0.118	0.109	0.065	0.014	0.017	0.017	4.719	4.742	5.075	−0.941	−0.726	−0.726	5.156	5.188	5.437	−0.900	−0.690	−0.690
								(1.103)	(1.098)	(1.075)	(0.953)	(0.944)	(0.944)	(1.205)	(1.201)	(1.151)	(0.912)	(0.897)	(0.897)
	$\frac{2}{3}$	0.289	0.268	0.155	0.024	0.029	0.029	4.967	4.980	5.246	−0.931	−0.715	−0.715	5.717	5.720	5.765	−0.881	−0.688	−0.688
								(1.161)	(1.153)	(1.111)	(0.943)	(0.930)	(0.930)	(1.336)	(1.325)	(1.221)	(0.893)	(0.895)	(0.895)

Table 12a. $F_{\mathrm{I}B,\infty}$, $(F_{\mathrm{II}B,\infty})$, $F_{\mathrm{I}B',\infty}(F_{\mathrm{II}B',\infty})$ and $F_{\mathrm{I}D,\infty}(F_{\mathrm{II}D,\infty})$ for a row of diamond-shaped inclusions (number of inclusion; $N \to \infty$) at the corner B, B' and D under various loading conditions. (Plane strain state $\nu_1 = \nu_2 = 0.3$). $F_{\mathrm{I}B,\infty} = F_{\mathrm{I},\lambda_1,k}$ at the corner B when $N \to \infty$.

(a) Uniaxial tension

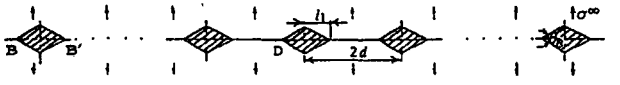

		$F_{\mathrm{I}B,\infty}(F_{\mathrm{I}B,\infty}/F_{\mathrm{I},\lambda_1}\|_{l_1/d=0})$						$F_{\mathrm{I}B',\infty}(F_{\mathrm{I}B',\infty}/F_{\mathrm{I},\lambda_1}\|_{l_1/d=0})$						$F_{\mathrm{I}D,\infty}(F_{\mathrm{I}D,\infty}/F_{\mathrm{I},\lambda_1}\|_{l_1/d=0})$					
G_2/G_1		10^{-5}	10^{-2}	10^{-1}	10^{1}	10^{2}	10^{5}	10^{-5}	10^{-2}	10^{-1}	10^{1}	10^{2}	10^{5}	10^{-5}	10^{-2}	10^{-1}	10^{1}	10^{2}	10^{5}
θ_B	$l_{1/d}$																		
30°	0	1.042	0.909	0.747	−0.160	−0.174	−0.177	1.042	0.909	0.747	−0.160	−0.174	−0.177	1.042	0.909	0.747	−0.160	−0.174	−0.177
		(1.000)	(1.000)	(1.000)	(1.000)	(1.000)	(1.000)	(1.000)	(1.000)	(1.000)	(1.000)	(1.000)	(1.000)	(1.000)	(1.000)	(1.000)	(1.000)	(1.000)	(1.000)
	$\frac{1}{3}$	1.063	0.957	0.754	−0.164	−0.178	−0.181	1.072	0.963	0.757	−0.165	−0.179	−0.192	1.093	0.975	0.763	−0.165	−0.184	−0.198
		(1.020)	(1.053)	(1.009)	(1.025)	(1.023)	(1.023)	(1.029)	(1.059)	(1.013)	(1.031)	(1.029)	(1.085)	(1.049)	(1.073)	(1.021)	(1.031)	(1.057)	(1.119)
	$\frac{1}{2}$	1.097	0.978	0.761	−0.166	−0.184	−0.186	1.121	1.001	0.770	−0.174	−0.191	−0.205	1.170	1.032	0.781	−0.176	−0.200	−0.219
		(1.053)	(1.076)	(1.019)	(1.038)	(1.057)	(1.051)	(1.076)	(1.101)	(1.031)	(1.088)	(1.098)	(1.158)	(1.123)	(1.135)	(1.046)	(1.100)	(1.149)	(1.237)
	$\frac{2}{3}$	1.147	1.014	0.769	−0.169	−0.192	−0.213	1.223	1.082	0.799	−0.186	−0.213	−0.226	1.329	1.141	0.815	−0.194	−0.229	−0.263
		(1.101)	(1.116)	(1.029)	(1.056)	(1.103)	(1.203)	(1.174)	(1.190)	(1.070)	(1.163)	(1.224)	(1.277)	(1.275)	(1.255)	(1.091)	(1.213)	(1.316)	(1.486)
60°	0	1.148	1.054	0.717	−0.154	−0.173	−0.175	1.148	1.054	0.717	−0.154	−0.173	−0.175	1.148	1.054	0.717	−0.154	−0.173	−0.175
		(1.000)	(1.000)	(1.000)	(1.000)	(1.000)	(1.000)	(1.000)	(1.000)	(1.000)	(1.000)	(1.000)	(1.000)	(1.000)	(1.000)	(1.000)	(1.000)	(1.000)	(1.000)
	$\frac{1}{3}$	1.169	1.082	0.728	−0.168	−0.188	−0.188	1.175	1.086	0.730	−0.172	−0.189	−0.194	1.192	1.110	0.734	−0.174	−0.194	−0.199
		(1.018)	(1.027)	(1.015)	(1.091)	(1.087)	(1.074)	(1.024)	(1.030)	(1.018)	(1.117)	(1.092)	(1.109)	(1.038)	(1.053)	(1.024)	(1.130)	(1.121)	(1.137)
	$\frac{1}{2}$	1.198	1.100	0.734	−0.175	−0.194	−0.195	1.217	1.122	0.742	−0.186	−0.209	−0.213	1.264	1.170	0.756	−0.192	−0.218	−0.228
		(1.044)	(1.044)	(1.024)	(1.136)	(1.121)	(1.114)	(1.060)	(1.065)	(1.035)	(1.208)	(1.208)	(1.217)	(1.101)	(1.110)	(1.054)	(1.247)	(1.260)	(1.303)
	$\frac{2}{3}$	1.248	1.140	0.743	−0.183	−0.205	−0.210	1.315	1.208	0.775	−0.216	−0.250	−0.262	1.421	1.293	0.800	−0.228	−0.268	−0.280
		(1.087)	(1.082)	(1.036)	(1.188)	(1.185)	(1.200)	(1.145)	(1.146)	(1.081)	(1.403)	(1.445)	(1.497)	(1.238)	(1.227)	(1.116)	(1.481)	(1.549)	(1.600)
90°	0	1.293	1.223	0.858	−0.131	−0.148	−0.152	1.293	1.223	0.858	−0.131	−0.148	−0.152	1.293	1.223	0.858	−0.131	−0.148	−0.152
		(1.000)	(1.000)	(1.000)	(1.000)	(1.000)	(1.000)	(1.000)	(1.000)	(1.000)	(1.000)	(1.000)	(1.000)	(1.000)	(1.000)	(1.000)	(1.000)	(1.000)	(1.000)
	$\frac{1}{3}$	1.307	1.241	0.864	−0.154	−0.168	−0.168	1.307	1.242	0.864	−0.161	−0.177	−0.177	1.319	1.251	0.869	−0.169	−0.187	−0.189
		(1.011)	(1.015)	(1.007)	(1.176)	(1.135)	(1.105)	(1.011)	(1.016)	(1.007)	(1.229)	(1.196)	(1.164)	(1.020)	(1.023)	(1.013)	(1.290)	(1.264)	(1.243)
	$\frac{1}{2}$	1.334	1.266	0.873	−0.163	−0.181	−0.181	1.342	1.274	0.877	−0.191	−0.214	−0.217	1.385	1.306	0.890	−0.205	−0.231	−0.236
		(1.032)	(1.035)	(1.017)	(1.244)	(1.223)	(1.191)	(1.038)	(1.042)	(1.022)	(1.458)	(1.446)	(1.428)	(1.071)	(1.068)	(1.037)	(1.565)	(1.561)	(1.553)
	$\frac{2}{3}$	1.385	1.314	0.891	−0.178	−0.199	−0.201	1.439	1.370	0.921	−0.245	−0.289	−0.305	1.553	1.444	0.950	−0.268	−0.316	−0.317
		(1.071)	(1.074)	(1.038)	(1.359)	(1.345)	(1.322)	(1.113)	(1.120)	(1.073)	(1.870)	(1.953)	(2.007)	(1.201)	(1.181)	(1.107)	(2.046)	(2.135)	(2.086)

Table 12b. $F_{\mathrm{I}B,\infty}$, $(F_{\mathrm{II}B,\infty})$, $F_{\mathrm{I}B',\infty}(F_{\mathrm{II}B',\infty})$ and $F_{\mathrm{I}D,\infty}(F_{\mathrm{II}D,\infty})$ for a row of diamond-shaped inclusions (number of inclusion; $N \to \infty$) at the corner B, B' and D under various loading conditions. (Plane strain state $\nu_1 = \nu_2 = 0.3$). $F_{\mathrm{I}B,\infty} = F_{\mathrm{I},\lambda_1,k}$ at the corner B when $N \to \infty$.

(b) Biaxial tension

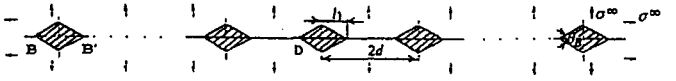

		$F_{\mathrm{I}B,\infty}(F_{\mathrm{I}B,\infty}/F_{\mathrm{I},\lambda_1}\|_{l_1/d=0})$						$F_{\mathrm{I}B',\infty}(F_{\mathrm{I}B',\infty}/F_{\mathrm{I},\lambda_1}\|_{l_1/d=0})$						$F_{\mathrm{I}D,\infty}(F_{\mathrm{I}D,\infty}/F_{\mathrm{I},\lambda_1}\|_{l_1/d=0})$					
G_2/G_1		10^{-5}	10^{-2}	10^{-1}	10^{1}	10^{2}	10^{5}	10^{-5}	10^{-2}	10^{-1}	10^{1}	10^{2}	10^{5}	10^{-5}	10^{-2}	10^{-1}	10^{1}	10^{2}	10^{5}
θ_B	$l_{1/d}$																		
30°	0	1.014	0.889	0.749	0.214	0.244	0.251	1.014	0.889	0.749	0.214	0.244	0.251	1.014	0.889	0.749	0.214	0.244	0.251
		(1.000)	(1.000)	(1.000)	(1.000)	(1.000)	(1.000)	(1.000)	(1.000)	(1.000)	(1.000)	(1.000)	(1.000)	(1.000)	(1.000)	(1.000)	(1.000)	(1.000)	(1.000)
	$\frac{1}{3}$	1.059	0.920	0.764	0.219	0.251	0.254	1.066	0.930	0.766	0.221	0.253	0.276	1.067	0.945	0.770	0.223	0.259	0.278
		(1.044)	(1.035)	(1.020)	(1.023)	(1.029)	(1.012)	(1.051)	(1.046)	(1.023)	(1.033)	(1.037)	(1.100)	(1.052)	(1.063)	(1.028)	(1.042)	(1.061)	(1.108)
	$\frac{1}{2}$	1.092	0.942	0.770	0.224	0.261	0.265	1.119	0.967	0.781	0.231	0.268	0.300	1.148	1.005	0.790	0.237	0.279	0.305
		(1.077)	(1.060)	(1.028)	(1.047)	(1.070)	(1.056)	(1.104)	(1.088)	(1.043)	(1.079)	(1.098)	(1.195)	(1.132)	(1.130)	(1.055)	(1.107)	(1.143)	(1.215)
	$\frac{2}{3}$	1.143	0.983	0.780	0.230	0.270	0.304	1.231	1.044	0.811	0.250	0.297	0.339	1.310	1.123	0.830	0.260	0.317	0.359
		(1.127)	(1.106)	(1.041)	(1.075)	(1.107)	(1.211)	(1.214)	(1.174)	(1.083)	(1.168)	(1.217)	(1.351)	(1.292)	(1.263)	(1.108)	(1.215)	(1.299)	(1.430)
60°	0	1.034	0.950	0.648	0.283	0.310	0.313	1.034	0.950	0.648	0.283	0.310	0.313	1.034	0.950	0.648	0.283	0.310	0.313
		(1.000)	(1.000)	(1.000)	(1.000)	(1.000)	(1.000)	(1.000)	(1.000)	(1.000)	(1.000)	(1.000)	(1.000)	(1.000)	(1.000)	(1.000)	(1.000)	(1.000)	(1.000)
	$\frac{1}{3}$	1.071	0.992	0.663	0.289	0.318	0.313	1.081	0.998	0.666	0.295	0.322	0.327	1.096	1.020	0.674	0.297	0.331	0.332
		(1.036)	(1.044)	(1.023)	(1.021)	(1.026)	(1.000)	(1.045)	(1.051)	(1.028)	(1.042)	(1.039)	(1.045)	(1.060)	(1.074)	(1.040)	(1.049)	(1.068)	(1.061)
	$\frac{1}{2}$	1.107	1.022	0.673	0.298	0.331	0.319	1.141	1.051	0.690	0.309	0.345	0.355	1.189	1.100	0.707	0.318	0.357	0.365
		(1.071)	(1.076)	(1.039)	(1.053)	(1.068)	(1.019)	(1.103)	(1.106)	(1.065)	(1.092)	(1.113)	(1.134)	(1.150)	(1.158)	(1.091)	(1.124)	(1.152)	(1.166)
	$\frac{2}{3}$	1.165	1.069	0.689	0.308	0.343	0.327	1.264	1.158	0.734	0.341	0.392	0.418	1.372	1.246	0.765	0.356	0.413	0.433
		(1.127)	(1.125)	(1.063)	(1.088)	(1.106)	(1.045)	(1.222)	(1.219)	(1.133)	(1.205)	(1.265)	(1.335)	(1.327)	(1.312)	(1.181)	(1.258)	(1.332)	(1.383)
90°	0	1.010	0.952	0.654	0.427	0.447	0.453	1.010	0.952	0.654	0.427	0.447	0.453	1.010	0.952	0.654	0.427	0.447	0.453
		(1.000)	(1.000)	(1.000)	(1.000)	(1.000)	(1.000)	(1.000)	(1.000)	(1.000)	(1.000)	(1.000)	(1.000)	(1.000)	(1.000)	(1.000)	(1.000)	(1.000)	(1.000)
	$\frac{1}{3}$	1.060	0.998	0.675	0.434	0.456	0.458	1.078	1.013	0.686	0.438	0.460	0.471	1.112	1.057	0.707	0.444	0.468	0.474
		(1.050)	(1.048)	(1.032)	(1.016)	(1.020)	(1.011)	(1.067)	(1.064)	(1.049)	(1.026)	(1.029)	(1.040)	(1.101)	(1.110)	(1.081)	(1.040)	(1.047)	(1.046)
	$\frac{1}{2}$	1.113	1.044	0.698	0.442	0.466	0.466	1.171	1.097	0.727	0.459	0.489	0.507	1.257	1.182	0.767	0.472	0.505	0.514
		(1.102)	(1.097)	(1.067)	(1.035)	(1.043)	(1.029)	(1.159)	(1.152)	(1.112)	(1.075)	(1.094)	(1.119)	(1.245)	(1.242)	(1.173)	(1.105)	(1.130)	(1.135)
	$\frac{2}{3}$	1.183	1.108	0.726	0.455	0.482	0.474	1.321	1.235	0.801	0.511	0.558	0.601	1.495	1.385	0.864	0.532	0.593	0.608
		(1.171)	(1.164)	(1.110)	(1.066)	(1.078)	(1.046)	(1.308)	(1.297)	(1.225)	(1.197)	(1.248)	(1.327)	(1.480)	(1.455)	(1.321)	(1.246)	(1.327)	(1.342)

Table 12c. $F_{\mathrm{I}B,\infty}$, $(F_{\mathrm{II}B,\infty})$, $F_{\mathrm{I}B',\infty}(F_{\mathrm{II}B',\infty})$ and $F_{\mathrm{I}D,\infty}(F_{\mathrm{II}D,\infty})$ for a row of diamond-shaped inclusions (number of inclusion; $N \to \infty$) at the corner B, B' and D under various loading conditions. (Plane strain state $\nu_1 = \nu_2 = 0.3$). $F_{\mathrm{I}B,\infty} = F_{\mathrm{I},\lambda_1,k}$ at the corner B when $N \to \infty$.

(b) Biaxial tension

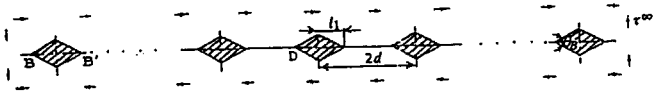

		$F_{\mathrm{II}B,\infty}(F_{\mathrm{II}B,\infty}/F_{\mathrm{II},\lambda_2}\|_{l_1/d=0})$						$F_{\mathrm{II}B',\infty}(F_{\mathrm{II}B',\infty}/F_{\mathrm{II},\lambda_2}\|_{l_1/d=0})$						$F_{\mathrm{II}D,\infty}(F_{\mathrm{II}D,\infty}/F_{\mathrm{II},\lambda_2}\|_{l_1/d=0})$					
G_2/G_1		10^{-5}	10^{-2}	10^{-1}	10^{1}	10^{2}	10^{5}	10^{-5}	10^{-2}	10^{-1}	10^{1}	10^{2}	10^{5}	10^{-5}	10^{-2}	10^{-1}	10^{1}	10^{2}	10^{5}
θ_B	$l_{1/d}$																		
30°	0	1.154	1.126	1.026	—	—	−0.584	1.154	1.126	1.026	—	—	−0.584	1.154	1.126	1.026	—	—	−0.584
		(1.000)	(1.000)	(1.000)			(1.000)	(1.000)	(1.000)	(1.000)			(1.000)	(1.000)	(1.000)	(1.000)			(1.000)
	$\frac{1}{3}$	1.185	1.153	1.044	—	—	−0.701	1.196	1.163	1.046	—	—	−0.703	1.224	1.192	1.066	—	—	−0.654
		(1.027)	(1.024)	(1.018)			(1.200)	(1.036)	(1.033)	(1.019)			(1.204)	(1.061)	(1.059)	(1.039)			(1.120)
	$\frac{1}{2}$	1.222	1.186	1.062	—	—	−0.738	1.268	1.227	1.089	—	—	−0.741	1.335	1.293	1.124	—	—	−0.640
		(1.059)	(1.053)	(1.035)			(1.264)	(1.099)	(1.090)	(1.061)			(1.269)	(1.157)	(1.148)	(1.096)			(1.096)
	$\frac{2}{3}$	1.284	1.243	1.091	—	—	−0.749	1.427	1.375	1.171	—	—	−0.755	1.568	1.501	1.236	—	—	−0.626
		(1.113)	(1.104)	(1.063)			(1.283)	(1.237)	(1.221)	(1.141)			(1.293)	(1.359)	(1.333)	(1.205)			(1.072)
60°	0	1.599	1.586	1.507	—	−0.721	−0.651	1.599	1.586	1.507	—	−0.721	−0.651	1.599	1.586	1.507	—	−0.721	−0.651
		(1.000)	(1.000)	(1.000)		(1.000)	(1.000)	(1.000)	(1.000)	(1.000)		(1.000)	(1.000)	(1.000)	(1.000)	(1.000)		(1.000)	(1.000)
	$\frac{1}{3}$	1.647	1.638	1.543	—	−0.762	−0.786	1.680	1.665	1.563	—	−0.764	−0.788	1.729	1.708	1.595	—	−0.737	−0.744
		(1.030)	(1.033)	(1.024)		(1.057)	(1.207)	(1.051)	(1.050)	(1.037)		(1.060)	(1.210)	(1.081)	(1.077)	(1.058)		(1.022)	(1.143)
	$\frac{1}{2}$	1.711	1.689	1.582	—	−0.768	−0.832	1.828	1.801	1.659	—	−0.771	−0.835	1.943	1.913	1.737	—	−0.720	−0.735
		(1.070)	(1.065)	(1.050)		(1.065)	(1.278)	(1.143)	(1.136)	(1.101)		(1.069)	(1.283)	(1.215)	(1.206)	(1.153)		(0.999)	(1.129)
	$\frac{2}{3}$	1.804	1.784	1.641	—	−0.798	−0.833	2.164	2.117	1.869	—	−0.804	−0.839	2.416	2.351	2.020	—	−0.694	−0.650
		(1.128)	(1.125)	(1.089)		(1.107)	(1.280)	(1.353)	(1.335)	(1.240)		(1.115)	(1.289)	(1.511)	(1.482)	(1.340)		(0.963)	(0.998)
90°	0	4.279	4.318	4.723	−0.987	−0.769	−0.769	4.279	4.318	4.723	−0.987	−0.769	−0.769	4.279	4.318	4.723	−0.987	−0.769	−0.769
		(1.000)	(1.000)	(1.000)	(1.000)	(1.000)	(1.000)	(1.000)	(1.000)	(1.000)	(1.000)	(1.000)	(1.000)	(1.000)	(1.000)	(1.000)	(1.000)	(1.000)	(1.000)
	$\frac{1}{3}$	4.469	4.494	4.874	−0.960	−0.743	−0.743	4.639	4.674	5.022	−0.956	−0.741	−0.741	4.822	4.829	5.161	−0.927	−0.713	−0.713
		(1.044)	(1.041)	(1.032)	(0.973)	(0.966)	(0.966)	(1.084)	(1.082)	(1.063)	(0.969)	(0.964)	(0.964)	(1.127)	(1.118)	(1.093)	(0.939)	(0.927)	(0.927)
	$\frac{1}{2}$	4.654	4.693	5.044	−0.932	0.715	−0.715	5.353	5.353	5.562	−0.918	−0.715	−0.715	5.794	5.795	5.915	−0.870	−0.658	−0.658
		(1.088)	(1.087)	(1.068)	(0.944)	(0.930)	(0.930)	(1.251)	(1.240)	(1.178)	(0.930)	(0.930)	(0.930)	(1.354)	(1.342)	(1.252)	(0.881)	(0.856)	(0.856)
	$\frac{2}{3}$	4.963	4.990	5.284	−0.898	−0.695	−0.695	6.902	6.870	6.687	−0.888	−0.700	−0.700	7.997	7.889	7.448	−0.801	−0.616	−0.616
		(1.160)	(1.156)	(1.119)	(0.910)	(0.904)	(0.904)	(1.613)	(1.591)	(1.416)	(0.900)	(0.910)	(0.910)	(1.869)	(1.827)	(1.577)	(0.812)	(0.801)	(0.801)

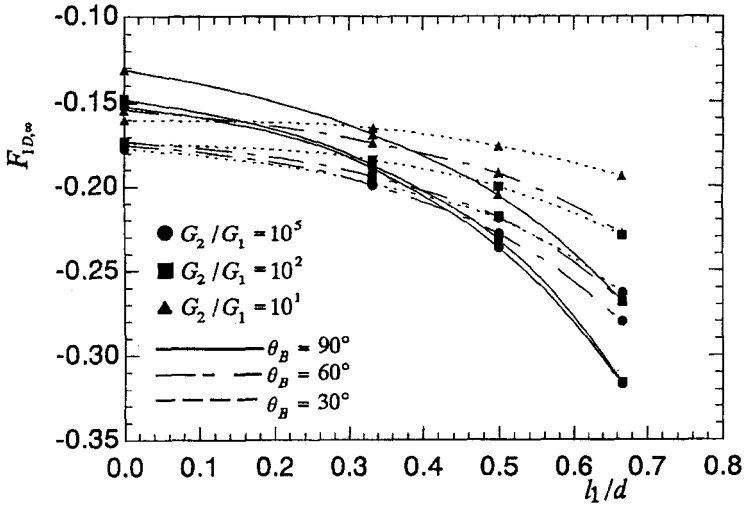

Figure 9. Interaction of $F_{1D,\infty}$ for a row of diamond-shaped inclusions at the corner D under uniaxial tension (y-direction). ($N \to infty, G_2/G_1 > 1$, plane strain state $\nu_1 = \nu_2 = 0.3$).

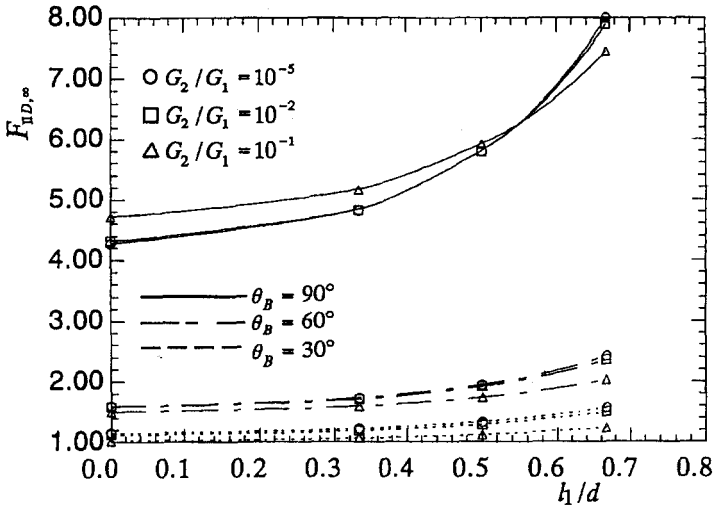

Figure 10. Interaction of $F_{IID,\infty}$ for a row of diamond-shaped inclusions at the corner D under in-plane shear. ($N \to \infty, G_2/G_1 < 1$, plane strain state $\nu_1 = \nu_2 = 0.3$).

occur at the outermost inclusions. Under in-plane shear as shown in Table 11(c), the maximum values occur at the central inclusions when $G_2/G_1 < 1$ and at the outermost inclusions when $G_2/G_1 > 1$. On the other hand, from Table 12 for $\theta_B \leq 90°$, under uniaxial tension (y-direction) (Table 12(a)) and biaxial tension (Table 12(b)), the maximum values always occur at the central inclusions. Under in-plane shear (Table 12(c)), the maximum values occur at the central inclusions when $G_2/G_1 < 1$ and at the outermost inclusions when $G_2/G_1 > 1$. In those Tables, the maximum values of $F_{\mathrm{I},\lambda_1,k}$ are shown for tension, and the maximum values of $F_{\mathrm{II},\lambda_2,k}$ are shown for in-plane shear.

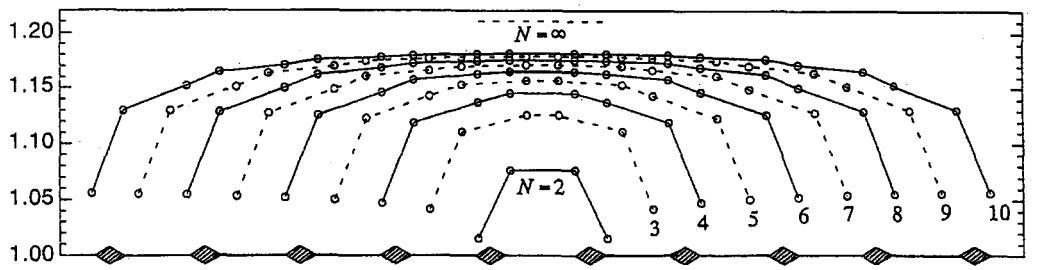

Figure 11. $F_{\mathrm{I},\lambda_1,k}/F_{\mathrm{I},\lambda_1}|_{l_1/d=0}$ for each diamond-shaped inclusion. ($\theta_B = 30°, l_1/d = \frac{2}{3}, G_2/G_1 = 10^1, \sigma_x^\infty = \sigma_y^\infty = \sigma^\infty, \tau_{xy}^\infty = 0$, plane strain state $\nu_1 = \nu_2 = 0.3$).

4. Conclusions

In this paper, interaction effects of stress intensity factors of angular corners were analyzed very accurately by using the singular integral equations of the body force method. The interaction effect of the angular corners was also discussed under various geometrical and loading conditions. The following conclusions can be drawn:

(1) In the numerical solution of the singular integral equations, the unknown functions were approximated by the products of the fundamental density functions and the power series. By examining the results of the various numbers, sizes, spacing and elastic parameters of inclusions, it was confirmed that the present method has good convergency of the numerical results by 4 digits when the number of collocation points around the corner is 12.

(2) The stress intensity factors of angular corners were found to be nearly linear with $1/N$ for fixed values of l_1/d or l_2/d. Based on this information, the stress intensity factors for $N \to \infty$ can be estimated.

(3) The interaction effect of a row of diamond-shaped inclusions was considered. Three fundamental types of loading conditions were discussed, (a) uniaxial tension, (b) biaxial tension and (c) in-plane shear. As a result, it was found that the interaction effect appears largely when the loading type is under uniaxial tension in y-direction, $\theta_B = 90°$ and $G_2/G_1 > 1$ ($F_{\mathrm{I},\lambda_1,k}$ at the corner D increases by about 100 percent), and when the loading type is in-plane shear, $\theta_B = 90°$ and $G_2/G_1 < 1$ ($F_{\mathrm{II},\lambda_2,k}$ at the corner D increases by about 80 percent).

(4) In a row of diamond-shaped inclusions of $\theta_A \leq 90°$, under uniaxial tension (x-direction), the maximum stress intensity factors occur at the outermost diamond-shaped inclusions when $G_2/G_1 < 1$ and at the central inclusions when $G_2/G_1 > 1$. Under biaxial tension, the maximum values occur at the outermost inclusions. Under in-plane shear, the maximum values occur at the central inclusions when $G_2/G_1 < 1$ and at the outermost inclusions when $G_2/G_1 > 1$.

(5) In a row of diamond-shaped inclusions of $\theta_B \leq 90°$, under uniaxial tension (y-direction) and biaxial tension, the maximum stress intensity factors always occur at the central inclusions. Under in-plane shear, the maximum values occur at the central inclusions when $G_2/G_1 < 1$ and at the outermost inclusions when $G_2/G_1 > 1$.

References

1. D.H. Chen and H. Nisitani, Stress Fields near the Corner of Jointed Dissimilar Materials. *Transactions of the Japan Society of Mechanical Engineers* 57-534 A(1991) 366–372 (in Japanese).

2. D.H. Chen and H. Nisitani, Analysis of Singular Stress Fields around a Corner Tip of Inclusion. *Transactions of the Japan Society of Mechanical Engineers* 57-542 A(1991) 2504–2508 (in Japanese).
3. D.H. Chen and H. Nisitani, Singular Stress Fields near the Corner of Jointed Dissimilar Materials. *Transactions of the ASME, Journal of Applied Mechanics* 60 (1993) 607–613.
4. D.H. Chen and H. Nisitani, Singular Stress Fields at Inclusion Corner. In Y. Fujitani, T. Miyoshi, and T. Taniguchi (eds), *Modelling, Computation and Analysis in Fracture Mechanics*, Kinokuniya (1994) pp. 93–113.
5. D.H. Chen, Stress intensity factors for V-notched strip under tension or in-plane bending. *International Journal of Fracture* 70 (1995) 81–97.
6. N.-A. Noda and K. Oda, Numerical solution of the singular integral equations in the crack analysis using the body force method. *International Journal of Fracture* 58 (1992) 285–304.
7. N.-A. Noda and K. Oda, Effect of curvature at the crack tip on the stress intensity factor for curved cracks. *International Journal of Fracture* 64 (1993) 239–249.
8. N.-A. Noda, K. Oda and T. Inoue, Analysis of newly-defined stress intensity factors for angular corners using singular integral equation of the body force method. *International Journal of Fracture* 76 (1996) 243–261.
9. M. Isida and H. Igawa, Some asymptotic behaviour and formulae of stress intensity factors for colinear and parallel cracks under various loadings. *International Journal of Fracture* 65 (1994) 247–259.
10. H. Nisitani, The two-dimentional stress problem solved using an electric digital computer. *Journal of the Japan Society of Mechanical Engineers* 70 (1967) 627–632. [Bulletin of *Japan Society of Mechanical Engineers* 11 (1968) 14–23.]
11. H. Nisitani, Solutions of notch problems by body force method. In G.C. Sih (ed.) *Mechanics of Fracture 5, Stress Analysis of Notched Problem*, Leyden (1978) pp. 1–68.